A SmallSat Concept to Resolve Diurnal and Vertical Variations of Aerosols, Clouds, and Boundary Layer Height

John E Yorks, Jun Wang, Matthew J Mcgill, Melanie Follette-Cook, Edward P Nowottnick, Jeffrey S Reid, Peter R Colarco, Jianglong Zhang, Olga Kalashnikova, Hongbin Yu, et al.

BAMS Article

A SmallSat Concept to Resolve Diurnal and Vertical Variations of Aerosols, Clouds, and Boundary Layer Height

John E. Yorks, Jun Wang, Matthew J. McGill, Melanie Follette-Cook, Edward P. Nowottnick, Jeffrey S. Reid, Peter R. Colarco, Jianglong Zhang, Olga Kalashnikova, Hongbin Yu, Franco Marenco, Joseph A. Santanello, Tammy M. Weckwerth, Zhanqing Li, James R. Campbell, Ping Yang, Minghui Diao, Vincent Noel, Kerry G. Meyer, James L. Carr, Michael Garay, Kenneth Christian, Angela Bennedetti, Allison M. Ring, Alice Crawford, Michael J. Pavolonis, Valentina Aquila, Jhoon Kim, and Shobha Kondragunta

ABSTRACT: A SmallSat mission concept is formulated here to carry out Time-varying Optical Measurements of Clouds and Aerosol Transport (TOMCAT) from space while embracing low-cost opportunities enabled by the revolution in Earth science observation technologies. TOMCAT's "around-the-clock" measurements will provide needed insights and strong synergy with existing Earth observation satellites to 1) statistically resolve diurnal and vertical variation of cirrus cloud properties (key to Earth's radiation budget), 2) determine the impacts of regional and seasonal planetary boundary layer (PBL) diurnal variation on surface air quality and low-level cloud distributions, and 3) characterize smoke and dust emission processes impacting their long-range transport on the subseasonal to seasonal time scales. Clouds, aerosol particles, and the PBL play critical roles in Earth's climate system at multiple spatiotemporal scales. Yet their vertical variations as a function of local time are poorly measured from space. Active sensors for profiling the atmosphere typically utilize sun-synchronous low-Earth orbits (LEO) with rather limited temporal and spatial coverage, inhibiting the characterization of spatiotemporal variability. Pairing compact active lidar and passive multiangle remote sensing technologies from an inclined LEO platform enables measurements of the diurnal and vertical variability of aerosols, clouds, and aerosol-mixing-layer (or PBL) height in tropical-to-midlatitude regions where most of the world's population resides. TOMCAT is conceived to bring potential societal benefits by delivering its data products in near–real time and offering on-demand hazard-monitoring capabilities to profile fire injection of smoke particles, the frontal lofting of dust particles, and the eruptive rise of volcanic plumes.

KEYWORDS: Boundary layer; Clouds; Remote sensing; Diurnal effects; Seasonal variability; Aerosols/particulates

https://doi.org/10.1175/BAMS-D-21-0179.1
Corresponding authors: John E. Yorks, john.e.yorks@nasa.gov; Jun Wang, jun-wang-1@uiowa.edu
Supplemental material: https://doi.org/10.1175/BAMS-D-21-0179.2

In final form 6 February 2023

AFFILIATIONS: Yorks, Follette-Cook, Nowottnick, Colarco, Yu, Santanello, and Meyer—NASA Goddard Space Flight Center, Greenbelt, Maryland; **Wang and McGill**—Department of Chemical and Biochemical Engineering, University of Iowa, Iowa City, Iowa; **Reid and Campbell**—U.S. Naval Research Laboratory, Monterey, California; **Zhang**—Department of Atmospheric Sciences, University of North Dakota, Grand Folks, North Dakota; **Kalashnikova and Garay**—Jet Propulsion Laboratory, California Institute of Technology, Pasadena, California; **Marenco**—Met Office, Exeter, United Kingdom, and The Cyprus Institute, Nicosia, Cyprus; **Weckwerth**—National Center for Atmospheric Research, Boulder, Colorado; **Li and Christian**—Earth System Science Interdisciplinary Center, and Department of Atmospheric and Oceanic Science, University of Maryland, College Park, College Park, Maryland; **Yang**—Department of Atmospheric Sciences, Texas A&M University, College Station, Texas; **Diao**—Department of Meteorology and Climate Science, San Jose State University, San Jose, California; **Noel**—Laboratoire d'Aérologie, CNRS/UPS, Observatoire Midi-Pyrénées, Toulouse, France; **Carr**—Carr Astronautics, Greenbelt, Maryland; **Bennedetti**—European Centre for Medium-Range Weather Forecasts, Reading, United Kingdom; **Ring**—Department of Atmospheric and Oceanic Science, University of Maryland, College Park, College Park, Maryland; **Crawford**—NOAA/Air Resources Laboratory, College Park, Maryland; **Pavolonis**—NOAA/Center for Satellite Applications and Research, Madison, Wisconsin; **Aquila**—Department of Environmental Science, American University, Washington, D.C.; **Kim**—Department of Atmospheric Sciences, Yonsei University, Seoul, South Korea; **Kondragunta**—NOAA/Center for Satellite Applications and Research, College Park, Maryland

Clouds and aerosol particles with strong diurnal processes play critical roles in Earth's hydrological, radiation, and air quality systems. Geostationary (GEO) sensors have long captured the significant horizontal and diurnal variability of clouds (Painemal et al. 2013; Delgado-Bonal et al. 2022), dust (Wang et al. 2003; Kondragunta et al. 2018), and fires/smoke (Zhang and Kondragunta 2008; Huff et al. 2021). However, GEO imagers provide high temporal resolution at the expense of vertical profiling, spatial resolution, and information content. While the GEO imagers for weather monitoring have similar capabilities, the GEO hyperspectrometers vary considerably in capability around the globe (Table ES1 in the online supplement; https://doi.org/10.1175/BAMS-D-21-0179.2). For example, the coverage and spatial resolution are 300–500 nm and 3.5 × 8 km^2, respectively, for Geostationary Environment Monitoring Spectrometer (GEMS), and 305–775 nm and 8 × 8 km^2 for Sentinel-4, and their algorithms for aerosol height retrievals are very different (Kim et al. 2019; Nanda et al. 2019; Chen et al. 2021).

The community also relies on a large cohort of polar, sun-synchronous, low-Earth-orbit (LEO) missions for global monitoring that, while providing excellent vertical profiling, spatial resolution, and information content, do not have the temporal sampling to statistically resolve the diurnal variability of cloud and aerosol fields, even at regional and seasonal scales, required to validate and improve aerosol transport, numerical weather, and climate model assumptions and skills. Data from the *Terra* and *Aqua* missions have led to >20,000 and >15,000 publications, respectively. To bridge the observation gap between GEO and LEO, the community is increasingly looking to develop affordable sensors that can be flown on multiple small satellites (as defined in Table ES2) as a constellation in LEO and launched via rideshare (multiple smaller-sized payloads can be transported to orbit on the same launch vehicle to reduce costs per payload). CubeSats are less than ~50,000 cm^3 in volume and <54 kg in mass, while SmallSats are up to 1,700,000 cm^3 in volume and 450 kg in mass and typically launch on an evolved expendable launch vehicle (EELV) secondary payload adapter (ESPA).

In the near future, there is a need for at least two types of missions: 1) the large or flagship missions with multiple sensors to extend the record of the cloud and aerosol for long-term climate monitoring and 2) new architectures that creatively utilize advanced SmallSat technologies to measure cloud and aerosol properties that are new or otherwise limited in spatial or temporal coverage, therefore offering constraints to both improve models and better interpret the climate data records generated in mission type 1. While a single SmallSat in a LEO has limited spatial coverage on the daily basis, the inclined orbit and synergistic imager/lidar data enable the diurnal variability of phenomena to be statistically resolved at regional and seasonal scales (Noel et al. 2018; Lee et al. 2019), as demonstrated in the "TOMCAT provides unprecedented sampling to statistically resolve diurnal variability at nearly global scale" sidebar.

Historically, flagship missions consisting of large sun-synchronous LEO satellites with large sensors have been the mainstay of global cloud and aerosol monitoring, starting with the Advanced Very High Resolution Radiometer (AVHRR) on NOAA satellites in late 1970s. NASA's Earth Observation System (EOS) followed in 2000 with the school-bus-sized *Terra* spacecraft (5,190 kg) and its Moderate Resolution Imaging Spectroradiometer (MODIS; King et al. 2013), Multiangle Imaging SpectroRadiometer (MISR; Diner et al. 1998), and Clouds and the Earth's Radiant Energy System (CERES) instruments. Placed in a polar orbit with a 1030/2230 local equatorial crossing time (LECT), *Terra* observations were intended to coincide with the minimum in daytime cloud cover and allowed for the first global daytime aerosol measurements. In 2002, the *Aqua* spacecraft (2,850 kg), with its own MODIS and CERES instruments joined *Terra* in EOS, creating a second set of observations at 0130/1330 LECT and forming the anchor of the NASA A-Train system. Like the *Terra* orbit, *Aqua* overpass time was strategically selected: any earlier it would simply repeat the MODIS *Terra* observations and have to cope with additional solar backscatter and glint, any later, and the scenes would be more dominated by cirrus shields from convection.

In the coming years, the A-Train hosted seven-member spacecraft, including a lidar on the *Cloud–Aerosol Lidar and Infrared Pathfinder Satellite Observations* (*CALIPSO*; Winker et al. 2009) and cloud radar on the *CloudSat* (Stephens et al. 2003) spacecraft allowing for day and night observations of the coupled cloud and aerosol system (635 and 995 kg, respectively). Future planned missions, such as ESA's upcoming EarthCARE with a lidar operating at a different wavelength (355 nm), will stay near the ~0130/1330 LECT to continue the multidecadal data record critical for Earth climate monitoring. While these active sensors provide detailed profiling information of aerosols and clouds, they only capture a small "snapshot" of the spatiotemporal variability due to limited spatial coverage (<1% of global surface) and constant LECT (Noel et al. 2018). Thus, even at seasonal and regional scales, consistent observations of the diurnal cycle of clouds and aerosols remain elusive, limiting publications that explore the diurnal variability of aerosol vertical distributions to only 80 (Table ES3), and numbers are similar for ice clouds and planetary boundary layer height (PBLH).

Given the strong scientific need to measure cloud and aerosol properties with improved spatial/temporal coverage and new affordable technologies that can be used synergistically to provide such observations, the cloud and aerosol communities can adopt recent strategies of the precipitation/convection community, which has already embraced the observing system concept of flagship LEO and GEO sensors supported by distributed SmallSats. For example, the convection and precipitation observing system consists of the flagship Global Precipitation Measurement (GPM; Hou et al. 2014) mission that utilizes larger passive microwave radiometer and radar remote sensors (3,850 kg satellite, with a 780 km radar and 150 kg radiometer). Representative examples of SmallSat instrument concepts that enable distributed architectures to target spatiotemporal variability and processes that are not observed by GPM, as discussed in Stephens et al. (2020), include the Temporal Experiment

for Storms and Tropical Systems Demonstration (TEMPEST-D) and RainCube. TEMPEST-D is a passive microwave radiometer that fits on a 6U CubeSat (as defined in Table ES2) and weighs only 14 kg (Reising et al. 2016). RainCube (12 kg total mass) is an atmospheric radar that utilizes a compact deployable antenna for compatibility with a 6U CubeSat platform (Peral et al. 2019). The Investigation of Convective Updrafts (INCUS) mission (launch is 2026), recently selected under the Earth Venture Mission (EVM-3), will utilize these technologies in a distributed architecture to obtain time-difference estimates of convective vertical motion that will enable the community to relate subdaily convective processes and dynamics to precipitation measurements from GPM. Furthermore, the Time-Resolved Observations of Precipitation structure and storm Intensity with a Constellation of SmallSats (TROPICS) mission comprises four CubeSats, each hosting a passive microwave spectrometer, in three low-Earth orbital planes to provide observations of tropical cyclones at high temporal resolution (Blackwell et al. 2018).

To our knowledge, there has not been a mission designed for a SmallSat that carries both active and passive sensors, in a distributed architecture or otherwise, to profile the distribution of aerosols and clouds at time-varying manner (different local times). This is primarily due to the challenges of reducing hardware size, mass, and cost while simultaneously maintaining the performance requirements for a backscatter lidar system. Smaller lidar and imager technologies are needed to provide synergic data that either augment our capability or provide the constraint to improve the retrieval of cloud-top height and other height information (such as for thick dust plumes) from infrared channels of GEO imagers in both day and night.

We present a single platform SmallSat mission concept that pairs a compact backscatter lidar ("TOMCAT uses four techniques for cloud, aerosol, and PBL height estimates" sidebar)

TOMCAT uses four techniques for cloud, aerosol, and PBL height estimates

The combination of passive multiangle and multiband observations with active lidar measurements on the same platform enables, for the first time, intercomparison and evaluation of four different techniques to "map" cloud, aerosol, and PBL heights across the ~450 km imager swath. These four techniques have heritage from the following proven algorithms (Fig. SB1): 1) a threshold-based profiling technique similar to CATS (Yorks et al. 2021) and *CALIPSO* (Vaughan et al. 2009), 2) stereo imaging using coincident visible measurements from LEO and GEO sensors, respectively, at different view angles (Carr et al. 2019, 2018), 3) MISR-like stereo height retrievals from three 26°-separated view angles (Mueller et al. 2017; Nelson et al. 2013), and 4) oxygen (O_2) B-band technique to determine the aerosol optical centroid height (AOCH) (Chen et al. 2021; Xu et al. 2017, 2019).

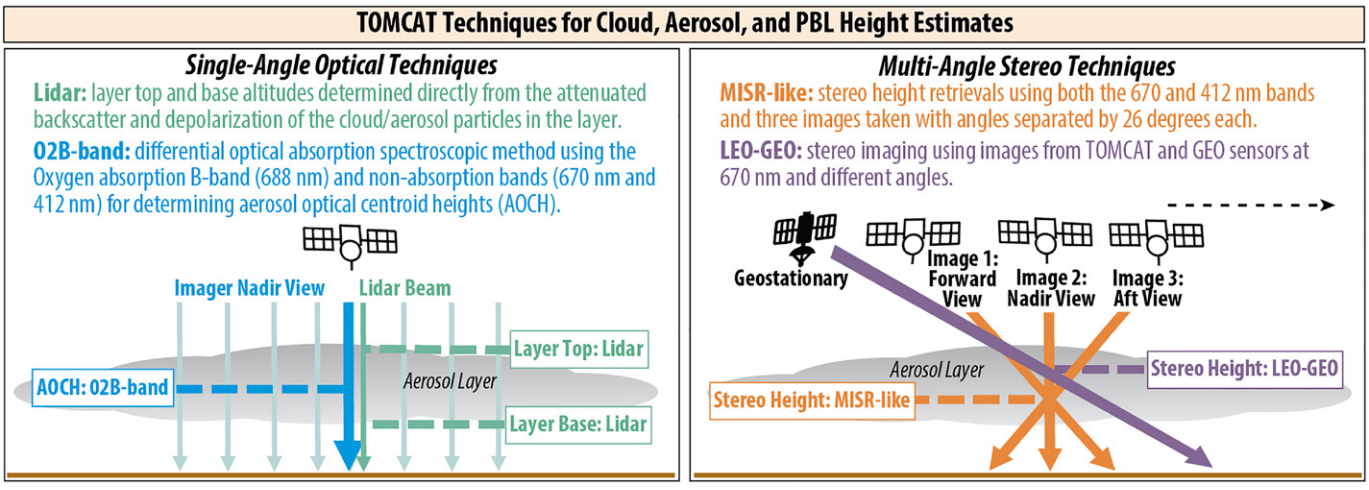

Fig. SB1. TOMCAT provides a comprehensive dataset of cloud, aerosol, and PBL heights by combining four different techniques, enabled by the coincident lidar and multiangle imager data. (left) The lidar provides the top and base height of atmospheric layers (green), while the O_2 B band enables estimates of the AOCH (blue). (right) Two stereo techniques are employed: a MISR-like multiangle method (orange) and a LEO–GEO method (purple).

The stereo height and AOCH generally correspond to the top height and central height of the aerosol layer, respectively, thereby providing complementary information to characterize aerosol vertical distribution. Hereafter, the stereo heights for aerosols and clouds are referred to as aerosol plume height (often but not necessarily always above the PBLH) and cloud-top height, respectively. While the stereo imaging method is robust for quantifying the height of aerosol plumes that are visibly heterogenous (i.e., near the source region), the O_2 B-band technique excels at retrieving AOCH for long-range transport cases (Xu et al. 2018). Furthermore, LEO–GEO and MISR-like stereo techniques complement each other through their respective strength in tackling the atmospheric motion vector (AMV) in the along-track and across-track directions, respectively, and they together provide better estimates of both AMV and cloud-top height or aerosol plume height at the same time (Horváth and Davies 2001; Mueller et al. 2017; Wu et al. 2009). The stereo technique, in comparison with other passive techniques, has a unique strength to derive the height of mid- and low-level clouds, including PBL clouds (Wu et al. 2009). All passive techniques can be refined and improved by collectively using lidar data to help classify the scenes dominated by PBL clouds.

with a passive multiangle imager in low-inclination orbit to obtain Time-varying Optical measurements of Clouds and Aerosol Transport (TOMCAT) in three dimensions. TOMCAT is designed to statistically resolve the vertical and diurnal variations of aerosols, clouds, and aerosol-mixing-layer height (AMLH), a proxy for the PBLH defined as the top of the mixing layer as observed by aerosol lidar data (Eresmaa et al. 2006; McGrath-Spangler and Denning 2013; Yang et al. 2013; Dang et al. 2019), as well as characterize the processes related to the diurnal evolution of aerosol emissions, cloud fraction, and cloud-top-layer height (Fig. 1). Please see an artist rendering of TOMCAT in Fig. ES1. Given the nature of turbulence associated with boundary layer process and the sporadic nature of dust and smoke emissions, the statistically resolved diurnal cycles therein are studied and described by TOMCAT to provide a strong constraint for numerical model predictions from the seasonal and regional point of view ("TOMCAT provides unprecedented sampling to statistically resolve diurnal variability at nearly global scale" sidebar).

The development of the TOMCAT lidar is a result of NASA Earth Science Technology Office (ESTO) investments in instrument capabilities and advances in SmallSat technologies. It provides the Earth science community with an affordable option for exploring the spatio-temporal variability of clouds and aerosol particles, particularly when (i) paired with a passive sensor that provides column measurements and cloud/aerosol heights over a swath and/or (ii) utilized in a distributed architecture of multiple copies flying in formation. TOMCAT has a strong heritage from and key differences with past and planned sensors. Its lidar concept stems from the Cloud–Aerosol Transport System (CATS; McGill et al. 2015; Yorks et al. 2016) that operated for 33 months on the International Space Station (ISS), providing vertical profiles

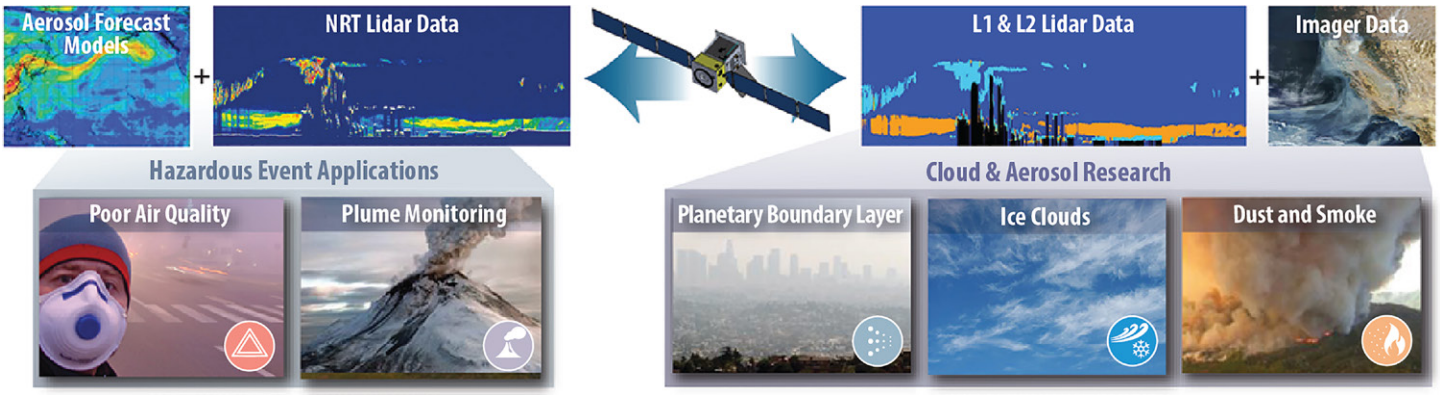

Fig. 1. Near-real-time lidar data products from TOMCAT, combined with aerosol forecast models, enable air quality forecasting and hazardous plume monitoring applications. The TOMCAT lidar and multiangle imager provide the data products necessary to achieve science objectives that advances our understanding of the diurnal and seasonal variability of aerosols, clouds, and PBL vertical structure. Icons (bottom-right corners in each panel of the second row) are used throughout the paper to highlight the mission's five themes/objectives.

TOMCAT provides unprecedented sampling to statistically resolve diurnal variability at nearly global scale

The TOMCAT mission concept enables the accurate statistical determination of the diurnal variability of aerosol, cloud, and PBL vertical structure that is representative of seasonal time scales and regional spatial scales (not diurnal variability within a single day). Several studies have shown that atmospheric reanalysis datasets and model parameterizations have large discrepancies (a factor of 2–3 depending on the local time and location) in the diurnal variation of PBLH, even at the season or annual scales (Liu and Liang 2010; Zhang et al. 2020). To demonstrate the TOMCAT sampling, we subsampled modeled atmospheric output from the NASA Goddard Earth Observing System, version 5 (GEOS-5), Nature Run along example TOMCAT orbit tracks at an hourly, 0.5° horizontal resolution for the period June–August 2006.

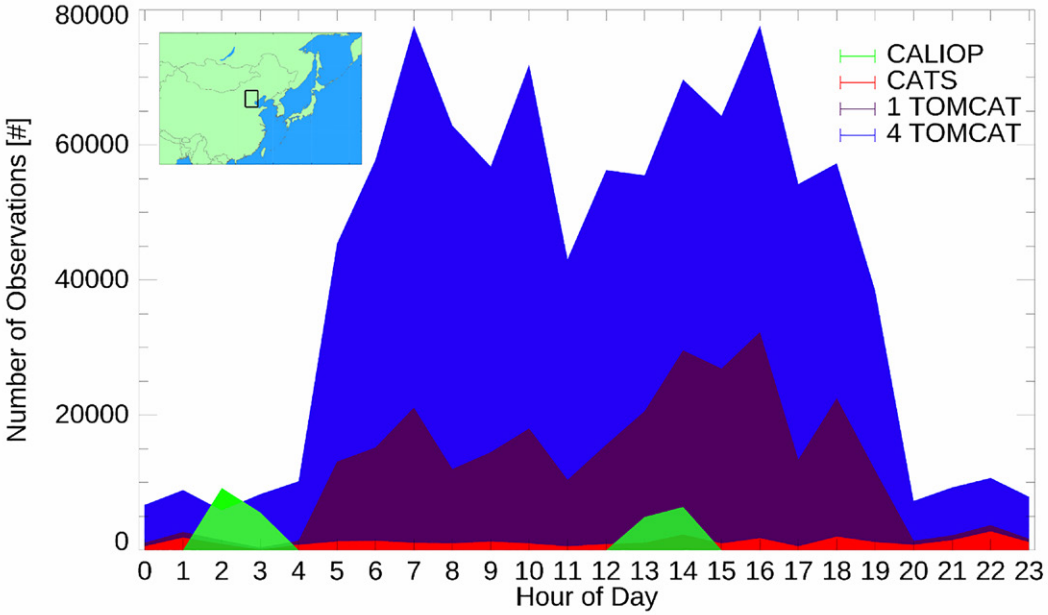

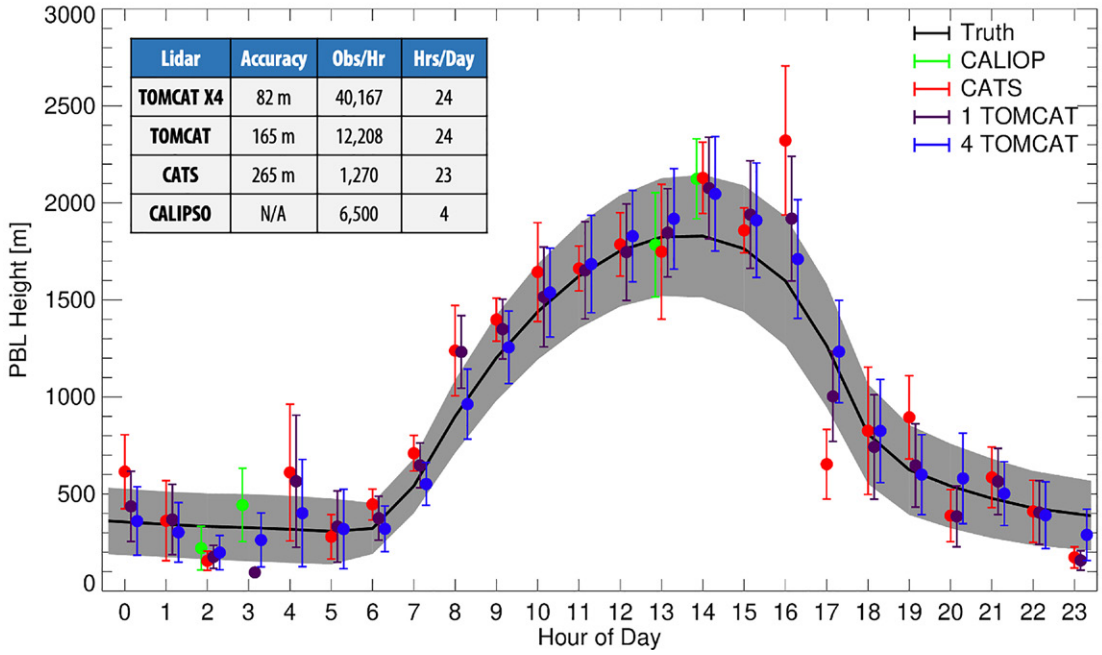

Fig. SB2. The TOMCAT mission concept provides data to statistically resolve the diurnal variability of PBLH on regional and seasonal scales. (top) For a 90-day period over a 5° latitude × 5° longitude grid box around Beijing, China (see inset), TOMCAT covers the entire diurnal cycle and provides more observations per hour than CATS and *CALIPSO*. (bottom) The TOMCAT spatiotemporal coverage also enables more accurate estimates of PBLH as a function of time of day.

The GEOS Nature Run was performed by the NASA Global Modeling and Assimilation Office (GMAO) (https://gmao.gsfc.nasa.gov/global_mesoscale/7km-G5NR/). The model output was constrained to conditions that represent high aerosol loading (AOD > 0.1) and clear sky (cloud fraction < 80%) because this is when the largest diurnal variability is expected.

Figure SB2 (top) shows that TOMCAT (purple) fully covers the entire diurnal cycle at an average rate of ~12,000 observations per hour in a season (90 days) and over a 5° × 5° grid box (comparable to the grid resolution of *CALIPSO* level-3 monthly products). To estimate the number of samples from each mission, we multiplied all 0.5° model records (~50 km) that are located in the 5° × 5° grid box by 10 to represent a 5 km along-track observation given that is the resolution of CATS and *CALIPSO* L2 data products (note that the TOMCAT concept L2 data products are at 3 km, but that is not considered for this sampling study). This provides a better estimate of the number of observations anticipated from TOMCAT compared to other lidar-related missions. The inclined orbit provides TOMCAT with 6 times more diurnal coverage compared to *CALIPSO*, which only provides data at 4 h day^{-1} (2–3 and 13–14 local hours) and the TOMCAT imager swath (450 km) creates 10 times more observations per hour than CATS (narrow 30 m curtain) during daytime hours.

The improved temporal sampling enables median hourly PBLH to be statistically resolved with an accuracy or root-mean-square error (RMSE) of 165 m over Beijing, China. The RMSE is computed by comparing the mean diurnal cycle of PBLH from each sensor to the mean diurnal cycle of the model truth within the 5° grid box around Beijing. Therefore, it does not include potential PBLH retrieval errors, just the error due to sampling with the TOMCAT mission concept. A concept that flies four copies of TOMCAT sensors (blue) in a 55° inclination orbit separated by 90° in the same orbital plane would further improve the ability to statistically retrieve the diurnal variability of PBLH on such a regional and seasonal scale. The increased sampling (~40,000 h^{-1}) compared to the single copy of TOMCAT yields further improvement in accuracy (RMSE of 82 m). Near-global PBLH climatologies such as the example in Fig. SB2 provide important context for the ground-based PBLH measurements that have finer temporal resolution (can resolve the diurnal variability on a single day) but have limited global coverage. Thus, an important aspect of achieving the TOMCAT science objectives would be combining these observations with ground-based PBL, aerosol, and cloud measurements.

of clouds and aerosols. CATS, like any space-based lidar, only provides measurements along the spacecraft track in a narrow footprint (~30 m).

To spread information across the satellite track, the lidar is paired with a multiangle imager that draws heritage from MISR measurements. This pairing enables the retrieval of stereo heights of clouds and aerosol plumes along a 400 km swath (Nelson et al. 2013) as well as estimates of the aerosol-layer height passively by using O_2 B bands (Chen et al. 2021; Xu et al. 2017, 2019). Unfortunately, MISR, *CALIPSO*, and CATS are on different satellite platforms with different orbits so their coincident measurements are scarce. To date, regardless of their wavelengths, a lidar and a visible multiangle imager capable of determining cloud and aerosol heights have not flown together in space. Although the NASA Earth System Observatory (ESO) Atmosphere Observing System (AOS) mission may fly a nearly identical SmallSat backscatter lidar in a 55° inclination orbit, the architecture is not final at this time and there are no plans for a collocated multiangle imager in the inclined orbit to improve spatiotemporal sampling.

Scientific and operational needs

Key properties of the atmosphere such as temperature, wind, and humidity exhibit strong variations throughout the day as a result of the diurnal variability of incoming solar radiation. These variations impact important processes such as surface–atmosphere exchange, aerosol life cycle (emission, dispersion, transport, and removal), and cloud formation. As such, the 2017–27 Decadal Survey for Earth Science and Applications from Space (ESAS 2017) highlighted the need for diurnally varying observations of clouds, aerosols, and the PBL following the National Academies of Sciences (NAS) recommendation (National Academies of Sciences, Engineering, and Medicine 2018).

Cirrus (high clouds) occur year-round, primarily over the tropics and midlatitudes, and have a significant influence on Earth's radiative balance (ESAS 2017 objective C-2a, "most important"). They are the most common cloud type observed in the atmosphere (40%–60% instantaneous global occurrence rates), and over half are translucent, making their altitude, amount, and optical properties very difficult to resolve with passive radiometric imagers and

active radar-based sensors (Mace et al. 2009). The sign of global net daytime radiative forcing for cirrus clouds is presently unknown, though ground-based lidar measurements suggest it may be a function of time of day (Campbell et al. 2016). Over many regions, particularly the tropics, cirrus occurrence is tied to convective processes triggered by solar input as a function of time (Sassen et al. 2009). Modern global models persistently show large discrepancies in diurnal cycle of clouds (DCC) and vertical distribution of clouds (VDC) for all clouds as a whole, in part due to the lack of observational constraints (Vignesh et al. 2020). For example, cloud-top height (CTH) is critically important for estimating cloud-top radiative cooling, but its retrieval shows significant differences among various passive remote sensing techniques; little is known about the variation of its retrieval uncertainty with the time of a day. Intrinsically coupled with strong diurnal cycle of solar radiation, the deficiency in simulating the phase and amplitude of the diurnal cycle of cloud fraction can lead to a systematic difference of ~2–3 W m^{-2} in net radiative energy at the top of atmosphere among different climate models (Yin and Porporato 2017). Furthermore, climate model simulations were previously found to underestimate ice water content (IWC) of cirrus clouds by a factor of 3–10 in the Northern Hemisphere when compared against aircraft observations (Patnaude et al. 2021). Due to the limited time-varying observations of IWC, model representations of diurnal differences in cirrus microphysical properties still require further investigation.

Aerosols, such as dust in arid regions and smoke particles in fire-prone regions and downwind areas, are responsible for poor air quality that causes millions of premature deaths every year and have significant ramifications for the health of the biosphere as well (Lelieveld et al. 2015; Murray et al. 2020). The magnitude of aerosol emissions for dust and smoke alike is typically determined by factors such as wind speed, temperature, humidity, atmospheric stability, soil moisture, and human activity and therefore are characterized by strong diurnal variability that are sometimes compounded with seasonal variabilities (as further discussed below). Interactions between aerosol emissions and the PBL determine aerosol transport and dispersion, with important implications for climate and air quality (ESAS 2017 objective W-5a, "most important"). Aerosols exhibit further spatiotemporal variability due to their diverse sources including windblown dust, wildfires, volcanic eruptions, fossil fuel combustion, and a variety of anthropogenic emissions. Two aerosol types that are important for long-range transport, desert dust and smoke from biomass burning, have emissions that are strongly affected by diurnally coupled meteorological processes (Wang et al. 2004, 2006; Giglio 2007; Andela et al. 2015; Lee et al. 2019; Yu et al. 2021). Recent analysis of CATS observations confirmed statistically significant diurnal variability in dust and dust mixture profiles over key dust sources, including the Bodélé depression, the West African El Djouf, the Rub' al-Khali desert, and western and southern North America driven by underlying meteorological processes in these regions (Wang et al. 2003; Lee et al. 2019; Yu et al. 2021). The dust emitted at various times of day is prominently transported across oceans and continents, providing key nutrients to marine and terrestrial ecosystems (i.e., soluble aerosols that are food for fish) and also causing poor air quality (Uno et al. 2009; Yu et al. 2012, 2015). Significant seasonal and diurnal variability in dust and dust mixture was identified in CATS observations over the vegetated regions in the Amazon and tropical southern Africa likely driven by enhanced dust emission due to wildfires (Yu et al. 2021). Biomass burning emissions also show substantial regionally dependent diurnal variability with daytime enhancements in wildfire burning intensity corresponding with increases in emissions and plume lofting (Seidel et al. 2012; Andela et al. 2015). A comparison of different chemistry transport models found differences as high as a factor of 10 in the vertical distribution of aerosols (Kipling et al. 2016), limiting the reliability of surface air quality estimates from space since aerosol optical depth retrieved widely from existing satellites is a columnar quantity.

Within the PBL (~from the surface up to ~0.5–3 km above Earth's surface), aerosol particles, also known as particulate matter (PM), are pollutants that cause poor-air-quality conditions harmful to human health (Li et al. 2017). Determining the effects of key diurnal PBL processes at minute to subseasonal time scales on air quality, weather prediction, and water cycle research was deemed a "most important" objective by ESAS (2017) (W-1a). PBLH and its spatiotemporal variability is a function of regional land and ocean characteristics, as well as seasonal atmospheric patterns (Holtslag et al. 2013; Baklanov et al. 2017). Furthermore, the PBL and its height vary considerably on time scales of an hour or less due to the diurnal cycle in solar heating (Molod et al. 2019; Wang and Christopher 2006), affecting the exchange of aerosols, water vapor, and energy with the free troposphere. In turn, PBLH can be defined from a backscatter lidar perspective as the top of the AMLH and/or top of PBL clouds (McGrath-Spangler and Denning 2013; Dang et al. 2019). This PBLH is an essential, diurnally dynamic aspect of Earth's coupled system that must be represented properly in weather, climate, and air quality forecast models to accurately predict the complex interactions between the surface (land and ocean) and the atmosphere (Esau and Zilitinkevich 2010; Holtslag et al. 2013). Thus, there is a need for observational global datasets suitable for evaluating and improving PBLH in weather and climate models (Shin et al. 2018). Measurements of AMLH/PBLH diurnal variability remain elusive outside of limited, point-based ground instruments and field campaigns (Molod et al. 2019; Seibert et al. 2000; Seidel et al. 2010; Shin et al. 2018). Additionally, global PBLH climatologies estimated from radiosonde data do not capture the diurnal variability due to the fixed launch times at 0000 and 1200 UTC each day.

Operationally, aerosol and AMLH monitoring are critical for a number of decision aids related to human health, transportation, and defense. Forecasting hazardous air quality and hazardous plume events is traditionally a function of national weather or environmental agencies, and has been typically performed with regional-scale models. Increasingly, global near-real-time aerosol forecasts are being produced by major international weather forecasting agencies and research institutions (Xian et al. 2019), opening a pathway to more accurately conveying information about intercontinental transport of aerosol plumes. These forecast models rely on near-real-time (NRT) observations for generating forecast initial conditions through data assimilation. Case studies assimilating lidar vertical profiles show a 20%–40% improvement in the simulation of volcanic plume distributions, aerosol backscatter, aerosol number concentration, and surface mass concentrations (Escribano et al. 2022; Ye et al. 2021; El Amraoui et al. 2020; Hughes et al. 2016; Sekiyama et al. 2010; Zhang et al. 2011). Operational and quasi-operational global aerosol models do not currently assimilate lidar vertical profiles since data are not available in NRT and the data lack the spatiotemporal information needed to improve model predictions on a global scale (Benedetti et al. 2018).

The TOMCAT SmallSat mission

The TOMCAT mission concept falls into the "new architectures that creatively utilize advanced SmallSat technologies" category discussed earlier in the paper, yet directly responds to emergent scientific and observation needs of the diurnal and vertical distribution of aerosol and cloud properties. Both the lidar and the imager fit on a SmallSat that is smaller than a household refrigerator and weighs about 300 kg. While many possible mission concepts can be formulated for such instruments, this single platform SmallSat mission concept costs less than $200 million (e.g., the approximate cap for PI-led NASA Earth Venture Mission), a sharp contrast from recent flagship missions such as *ICESat-2* (Markus et al. 2017), which cost about $1 billion and weighs ~1,500 kg. This TOMCAT concept addresses three scientific questions that are articulated in the sections above, including (i) How do the vertical and diurnal variability of ice cloud properties affect Earth's radiation budget? (ii) How do changes in PBLH with local time influence regional and seasonal surface air quality and

low-level cloud distributions? (iii) How do smoke and dust emission processes impact their atmospheric distributions and long-range transport on subseasonal (~2 weeks–2 months) to seasonal time scales (~2–4 months)? It will be equipped with NRT capabilities to uniquely support operational hazardous plume monitoring, aerosol forecasting, and air quality (AQ) assessments. Figure 2 shows the science traceability matrix that links the measurement requirements to the science and application goals.

Science Goal & Enabled Applications	Science & Applications Objectives		Measurement Requirements: Physical Parameters	Measurement Requirements: Observables	Instrument Requirements		Projected Performance	Mission Requirements (Top Level)
Science Goal: Advance our understanding of the diurnal and seasonal variability of aerosol, cloud, and PBL vertical structure that impact the Earth's energy balance, hydrological cycle, and air quality.	**S-1. Characterize seasonal and diurnal variability of cirrus ice cloud occurrence rates, vertical distributions, and optical scattering characteristics. *(2018 DSEOS C-2a)***	**Mapping of Science & Applications Objectives to Physical Parameters represented by icons**	**Cloud Top & Base Height**	Vertical Profiles of Attenuated Total Backscatter over the full 24-hour diurnal cycle in 90 days within a 5°x 5° grid box.	Lidar Backscatter Wavelengths	532 & 1064 nm	532 & 1064 nm	Operate the lidar instrument day and night.
			Aerosol Plume Height		Lidar Vert. & Hori. Resolution	<100 m (vert.) <500 m (hori.)	60 m (vert.) 478 m (hori.)	Near-nadir primary view with geo-referencing accuracy of <500 m.
					532 nm Telescope Field-Of-View (FOV)	<200 μradians	85 μradians	
	S-2. Quantify the diurnal, regional, and seasonal variability of PBL clouds and aerosol mixing layer heights. *(2018 DSEOS W-1a)*		**PBL Height**		Vertical Data Collection Range	>30 km	37.5 km	Operate the payload at LEO orbit to meet SNR and resolution requirements.
					Calibration Uncertainty	<10%	3-8% (532) 5-10% (1064)	
			Extinction Coefficient		Calibration Resolutions (SNR >75)	<1500 km (hori.) <5 km (vert.)	750 km (hor.) 2.5 km (vert.)	Orbit inclination that provides measurements over the full 24-hour diurnal cycle in 90 days within a 5° x 5° grid box.
					532 nm SNR in Aerosol Layer (AOD=0.10)	>2.00	6.82 (night) 3.28 (day)	
	S-3. Quantify the diurnal variability of mineral dust production and smoke injection heights on sub-seasonal to seasonal timescales. *(2018 DSEOS W-5a)*		**Ice Water Content**		532 nm Minimum Detectable Backscatter	<8.0E-4	4.1E-4 (night) 5.3E-4 (day)	
			Particle Sphericity	Vertical Profiles of Depolarization Ratio over the full 24-hour diurnal cycle in 90 days within a 5°x 5° grid box.	Lidar Depolarization Wavelengths	532 & 1064 nm	532 & 1064 nm	Operate for 2 years to observe two full seasonal cycles.
			Cloud Phase		Depolarization Purity	>100:1	~150:1	Produce and distribute >80% of lidar data within 6 hours of collection to applications end users.
			Aerosol Type		Depolarization Ratio Uncertainty	<100%	5-30% (night) 30-100% (day)	
Enabled Applications: Improved air quality and hazardous plume monitoring and forecasting.	**A-1. Provide aerosol vertical profiles to enable improved analysis and prediction of aerosol transport and air quality through data assimilation.**		**Aerosol Plume Height AOCH**	Multi-angle Radiance over the full 24-hour diurnal cycle in 90 days within a 5°x 5° grid box.	Imager Swath	>250 km	457 km	Target up to 2 hazardous events per week and perform 5-10 off-nadir pointing maneuvers per week.
					Band Wavelengths	Blue (400-500 nm) Red (600-700 nm) O_2 B-band	412.5 ± 7.5 nm 670 ± 10 nm 688 ± 0.5 nm	
					Nadir Pixel Resolution	<500 m	408 m	
	A-2. Determine aerosol injection heights, enabling improved modeling and monitoring of hazardous plume transport.		**Cloud Top Height**		Number of Angles	3	3	Operate the imager during daytime on same platform as the lidar instrument.
					SNR (at 3.3 km pixel res.)	>78 (412 nm) >128 (670 nm) >200 (688 nm)	>1094 (412 nm) >1115 (670 nm) >212 (688 nm)	
					Radiometric Calibration Uncertainty	<5%	3-5%	

Lidar-Related Requirements | Imager-Related Requirements

Fig. 2. The TOMCAT science traceability matrix provides a clear and concise tracking of instrument and mission requirements back to the science objectives. The three TOMCAT science objectives all trace back to the 2017–27 Decadal Survey for Earth Science and Applications from Space (National Academies of Sciences, Engineering, and Medicine 2018), as highlighted in paratheses after the objective text. Requirements are based on TOMCAT simulations and heritage from CATS, *CALIPSO*, and different passive sensors as discussed in the text.

TOMCAT data will be instrumental to fill gaps in our understanding of time-varying vertical profiles of ice clouds, aerosol particles (anthropogenic pollution, volcanic, smoke, dust), and PBLH. Data will also be provided in NRT for improving prediction of air quality and hazardous plumes from fires and volcanic eruptions in the tropics and midlatitudes. TOMCAT utilizes a straightforward implementation of a commercial SmallSat carrying a lidar and an imager. The TOMCAT lidar, a compact version of the CATS instrument, employs photon counting detection and a high-repetition-rate laser that continuously operates at 532 and 1,064 nm to measure backscatter and depolarization at both wavelengths. The TOMCAT imager consists of three cameras that provide radiance measurements at three angles separated by 26° and three bands (412, 670, 688 nm) with a swath width of ~450 km and a nadir pixel resolution of ~400 m. The spacecraft is in a 50°–55° inclination orbit to provide comprehensive spatial and temporal coverage of the tropics and midlatitudes covering over 97% of Earth's population. The low orbit altitude (400–450 km) maximizes the lidar signal-to-noise ratio (SNR), while the multiple-angle imager with O_2 B band improves the spatial converge of aerosol and cloud height retrievals ("TOMCAT uses four techniques for cloud, aerosol, and PBL height estimates" sidebar). The O_2 B band is selected because vegetated surface reflectance is low at this band and it is sensitive to the change of both thick and thin aerosol-layer height ("TOMCAT uses four techniques for cloud, aerosol, and PBL height estimates" sidebar). These mission characteristics enable TOMCAT to statistically resolve the diurnal variability of the vertical structure of cloud, aerosol, and AMLH at unprecedented accuracy and temporal coverage compared to previous lidar-based missions ("TOMCAT provides unprecedented sampling to statistically resolve diurnal variability at nearly global scale" sidebar). The TOMCAT data latency (<4 h) enables the data to be ingested into forecast models to improve the skill of hazardous air quality and aerosol plume forecasts.

The TOMCAT instrument design and feasibility

SmallSat lidar with on-demand pointing. Stephens et al. (2020) reported that over the past decade previous publications have referred to lidar technologies on a SmallSat as infeasible (Selva and Krejci 2012) and problematic (Selva and Krejci 2012). However, technology advances have yielded the TOMCAT lidar design that fits the mass (<120 kg), volume (<1.0 m^3), and power (<475 W) constraints of a SmallSat (Fig. 3), yet adds capabilities and improves performance compared to previous space-based lidars ("Compact, SmallSat lidar with added capabilities and better performance" sidebar). Many lidar concepts are designed to rely on big laser pulse energies (typically with low laser repetition rate) to overcome the noise floor of the detector, thereby having power requirements that are incompatible with a SmallSat implementation. In contrast, the TOMCAT lidar uses a high repetition rate, low pulse energy

Fig. 3. A half-scale printed model of the TOMCAT payload demonstrates fit and assembly of the SmallSat ESPA Grande package. (left) The laser (orange) is attached to the bottom panel of the instrument. (center) The telescope (yellow) and detectors (red and green) are shown in the fully assembled instrument, while (right) the electronics cards are shown on the side panel. The panels are clear in this 3D printed model, but the actual panels are made of M55J composite over an aluminum core.

Compact, SmallSat lidar with added capabilities and better performance

The TOMCAT lidar utilizes an affordable, low-risk standard backscatter lidar while leveraging the technology and algorithm heritage of CATS and *CALIPSO*, yet advances current capabilities (Table SB1) and performance (Fig. SB3) of these space-based lidars to provide essential data about cloud and aerosol heights and properties. To detect faint aerosol layers and optically thin cirrus clouds over all hours of the day, the TOMCAT lidar is designed to have higher daytime SNR than *CALIPSO* and CATS, as well as a minimum detectable backscatter (MDB; the backscatter at which the weakest atmospheric feature can be detected) at 532 nm at night and day that is better than the 532 nm nighttime MDB for CALIOP (<8.0×10^{-4} km^{-1} sr^{-1} for cirrus cloud between 10 and 12 km).

Table SB1. TOMCAT has more capabilities than previous space-based lidars and better MDB than *CALIPSO*. An asterisks indicates values from McGill et al. (2007). A hat/caret indicates CATS 532 nm values for mode 7.1 as reported by Yorks et al. (2016).

Capability	TOMCAT	*CALIPSO*	CATS
532 nm backscatter	✓	✓	
1,064 nm backscatter	✓	✓	✓
532 nm depolarization	✓	✓	
1,064 nm depolarization	✓		✓
<6 h data latency	✓		✓
Inclined orbit	✓		✓
Off-nadir pointing	✓		
532 MDB, day (km^{-1} sr^{-1})	5.30×10^{-4}	1.70×10^{-3}*	2.20×10^{-2}^
532 MDB, night (km^{-1} sr^{-1})	4.10×10^{-4}	8.00×10^{-4}*	1.0×10^{-3}^

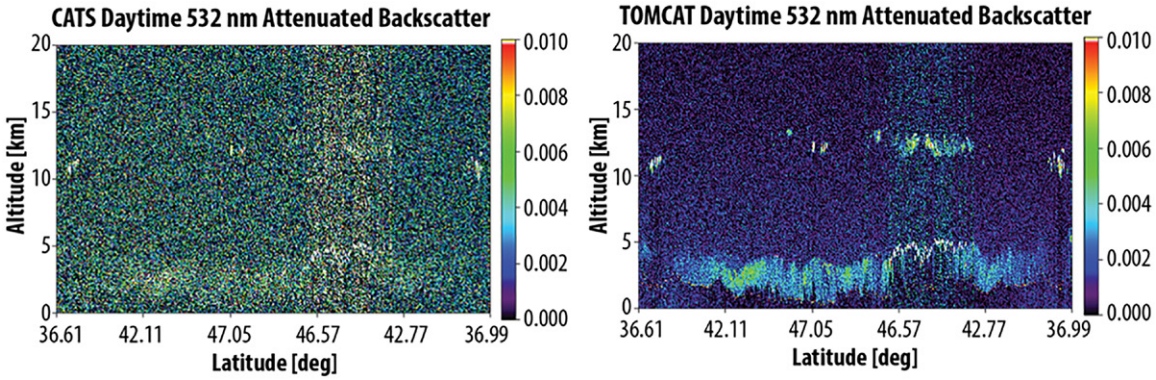

Fig. SB3. Simulations of daytime 532 nm attenuated total backscatter for (left) CATS and (right) TOMCAT demonstrate the 3-times-better SNR of the TOMCAT lidar compared to CATS, which improves layer detection. The simulated scene is from airborne CPL data of smoke and clouds over Idaho and Nevada (18 Aug 2015).

Simulations of the TOMCAT lidar were performed using the GSFC backscatter lidar simulator, developed for CATS prelaunch testing and algorithm development. Instrument specifications (Table 1) are used to simulate raw photon counts with random Poisson noise and solar background counts computed over different surface types and viewing conditions. The atmospheric state (i.e., profiles of extinction and backscatter) can be initialized using aircraft/ground-based data, GEOS model scenes, or simplified canonical cases. Observables such as total attenuated backscatter are then determined with systematic uncertainties (e.g., calibration uncertainty) using the lidar equation. The simulator has been verified against CATS data and by other institutions as part of AOS mission development work.

The TOMCAT lidar has 2–3-times-higher 532 nm SNR than *CALIPSO* and CATS at daytime, as shown in Fig. SB3. This enhanced SNR is primarily due to 2- and 3.6-times-more laser power than CATS and *CALIPSO*, respectively, and a ~35% lower orbit altitude than *CALIPSO*. The TOMCAT lidar will measure 532 nm backscatter (at raw resolutions) within a smoke aerosol layer (AOD = 0.10) between 0 and 2 km with an SNR of 6.82 (night) and 3.28 (day). The projected lidar SNR also results in 532 nm MDB (for cirrus cloud between 10 and 12 km) of 5.3×10^{-4} km^{-1} sr^{-1} during daytime operations and 4.1×10^{-4} km^{-1} sr^{-1} during night (Table SB3), ensuring TOMCAT will detect cloud, aerosol, and PBL heights accurately over all hours of the day. The TOMCAT lidar daytime 532 nm MDB, while not as good as its nighttime, will be better than CALIOP's *nighttime 532 nm MDB* (used for its layer detection algorithms).

laser operating in conjunction with photon-counting detectors. This approach offers significant advantages in the size, mass, and power required for the laser transmitter, while providing equivalent measurement sensitivity and spatial resolution. By integrating signals from multiple laser pulses, the measurement dynamic range is maintained. The Cloud Physics Lidar (CPL; McGill et al. 2002) instrument, with over 20 years of aircraft operation, and the CATS lidar have proven the high-repetition-rate, low-pulse-energy approach. Table 1 highlights the primary lidar instrument parameters. The SmallSat lidar design is mature as all components have CATS or other spaceflight heritage, or have undergone maturation and testing through NASA-funded technology investments. In addition, a life test is being conducted on the qualification laser, which began on 4 October 2020 and has continued since with no performance degradation.

Table 1. The TOMCAT lidar instrument parameters. The vertical and horizontal resolutions (see the last two rows) are easily adjusted to other values if desired/required by different science objectives.

Parameter	Value
Laser type	Nd:YVO4
Laser wavelengths	1,064 and 532 nm
Laser pulse energy	4 kHz
Laser pulse length	3 mJ (1,064 nm), 2 mJ (532 nm)
Transmitted beam divergence	70 μrad (1,064 nm), 35 μrad (532 nm)
Telescope diameter	60 cm
Telescope field of view	115 μrad (1,064 nm), 85 μrad (532 nm)
Vertical resolution	60 m
Horizontal resolution	16 Hz, 478 m

Multiangle observation imager. The multiple angle imaging techniques have been demonstrated by many satellite missions and therefore are relatively mature. Since the lidar drives the cost of TOMCAT, three commercial off-the-shelf cameras complete the TOMCAT instrument suite, complementing the lidar data with cloud and aerosol heights over a wide swath. Several flight-qualified and proven high-resolution cameras exist from commercial vendors that can provide a 55° × 55° FOV, corresponding to 1,944 × 1,944 pixels. Each camera operates over a specific wavelength band (405–420, 660–680, and 687.3–688.2 nm), using a commercial off-the-shelf bandpass filter. One possible candidate for such cameras would be the Malin Space Science Systems ECAM-50 wide FOV camera due to its modular, adaptable, high-reliability imaging system (Malin et al. 2010). Camera operation would be limited to beta angles between ±75. Each camera uses a standard 4.7 mm effective focal length (EFL), f/3.5 lens mounted to its detector, resulting in ~200 m nadir ground resolution in a ~450 km cross-track × ~450 km along-track image in a 400–450 km orbit. The camera images overlap every 26° so that as the spacecraft proceeds forward the nadir pixel of the current image falls on the 26° forward pixel of the previous image. Figure ES2 illustrates the measurement geometry, with images taken every 27.98 s, allowing ~47% image overlap. The blue (412 nm) and red (670 nm) bands have SNRs > 1,000, while O_2 B band (688 nm) has an SNR of >200, all at a 3.3 km resolution after coadding, thereby enabling three different aerosol height estimates ("TOMCAT uses four techniques for cloud, aerosol, and PBL height estimates" sidebar). The imager and specifications presented here are just one way to provide wide-swath passive height retrievals that are complementary to the lidar data. Other passive concepts, such as tandem stereo cameras or a polarimeter, could also enable estimates of cloud and aerosol heights over a swath.

TOMCAT scientific data products, applications, and validation

Lidar level-1 and level-2 data products. The projected TOMCAT lidar archival level 1 (L1) and level 2 (L2) data products are demonstrated in Fig. 4 using CATS 1,064 nm nighttime data, which have very similar SNR to the expected TOMCAT nighttime performance. A full list of the data products, as well as their resolutions, uncertainties, and data processing

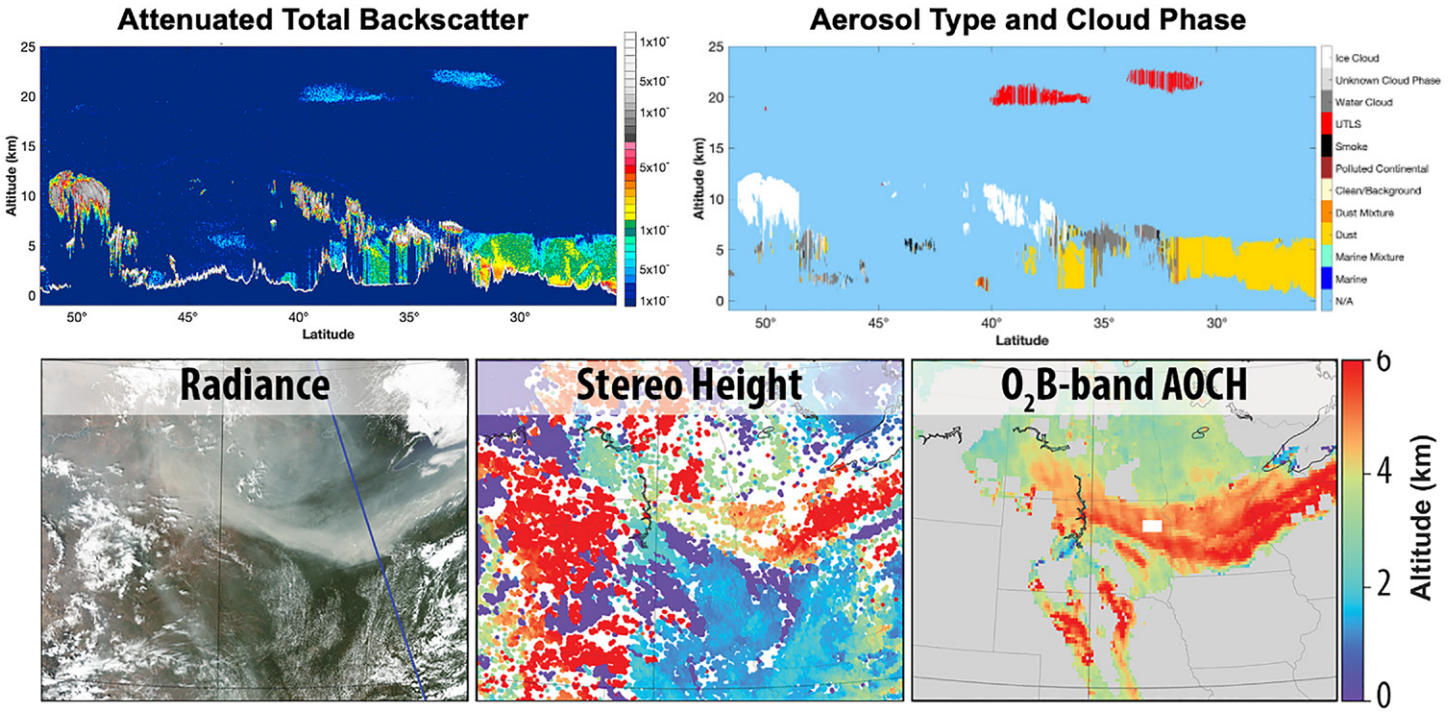

Fig. 4. Lidar level 1 data products include (top left) attenuated total backscatter and perpendicular backscatter at 532 and 1,064 nm (units: km^{-1} sr^{-1}). These products are used to create level 2 products such as (top right) aerosol type and cloud phase. The lidar data examples are CATS nighttime 1,064 nm attenuated total backscatter from 9 Sep 2017 over Central Asia and are representative of TOMCAT nighttime performance given the very similar nighttime 1064 nm SNRs between CATS and the TOMCAT lidar. (bottom) Also shown are the examples of synthetic data of TOMCAT imager data, including level-1B georeferenced radiance data, the stereo height data, and the AOCH data. Here, VIIRS, MISR, and TROPOMI data are used as the proxy for generating TOMCAT synthetic imager data. (bottom left) The image is rendered via three band overlays assuming that the data in green band, not available in TOMCAT imager, can be estimated from TOMCAT's blue and red bands, following the technique by Miller et al. (2012).

algorithms, are presented in Table ES4. These lidar data products and processing algorithms have robust heritage from CATS, *CALIPSO*, and the airborne CPL. The quality of the TOMCAT lidar data products are a function of the quality of the backscatter data, which is related to the SNR, MDB, and calibration uncertainty. The TOMCAT lidar design and algorithms result in backscatter calibration uncertainties of 3%–8% (532 nm) and 5%–10% (1,064 nm) using calibration techniques similar to CATS and *CALIPSO* (Getzewich et al. 2018; Kar et al. 2018; Pauly et al. 2019; Vaughan et al. 2019). L1 attenuated backscatter profiles are transformed into L2 data products such as layer heights (Yorks et al. 2021), PBLH (Palm et al. 2021), extinction coefficient (Young and Vaughan 2009; Hlavka et al. 2012), and IWC (Heymsfield et al. 2014) using heritage *CALIPSO* and CATS algorithms (Table ES4).

Imager level-1 and level-2 data products. The coincident multiangle and multiband measurements provided by the TOMCAT imager are highly complementary to the TOMCAT lidar data, enabling retrievals of cloud, aerosol, and PBL heights that augment the lidar's narrow footprint (~30 m) with a wide swath (~450 km) during the day. The imager provides visible radiances at three different angles that, with vicarious calibration (using a radiometrically stable calibration target such as the Libyan or White Sands deserts to monitor and correct for relative degradation), enable retrievals of cloud-top height and aerosol plume heights with an uncertainty of 100–200 m (Nelson et al. 2013; Carr et al. 2018, 2019), and the AOCH with an uncertainty of <500 m (Xu et al. 2017, 2019; Chen et al. 2021). Both AOCH and stereo height retrievals do not require onboard absolute calibration because the former depends on the ratio between O_2 B and its adjacent continuum band and the latter depends on the georeferenced feature contrast. Both retrievals can be evaluated using TOMCAT lidar

data, yielding important statistics when generating the lidar-imager synergistic L2 PBLH products. TOMCAT lidar depolarization ratios and multiangle images (from the cameras) can also help to separate nonspherical dust particles from spherical smoke particles, especially over the places such as northern Sahel and Australia region where dust and smoke coexist, and from spherical anthropogenic particles, especially over Asia (Omar et al. 2009; Nowottnick et al. 2022).

Level-3 synergistic data products for improved spatiotemporal sampling and resolving diurnal variability. TOMCAT combines lidar and passive stereo techniques to deliver near-global vertical and diurnal observations of aerosol, clouds, and PBL on seasonal to subseasonal time scales (via statistical averages for each hour). With an inclination angle of (50°–55°), the TOMCAT spacecraft orbits over the primary aerosol transport pathways, aerosol emission regions, midlatitude storm tracks, and tropical convection zones at a different local time each overpass. This sampling enables the diurnal variability of the geophysical variables to be statistically resolved; for each meteorological season (~90 days), the TOMCAT L2 data of cloud and aerosol occurrence, backscatter coefficient, extinction coefficient, and IWC can be gridded by region (i.e., 5° latitude × 5° longitude grid boxes), altitude (60 m bins), and hour of day (grid boxes can be modified based on the accuracy required for specific science targets). These measurements fundamentally challenge global atmospheric model development and provide novel constraints for model evaluation. We list some examples here:

- *Clouds*: Over many regions, and particularly the tropics that are the primary focus of the TOMCAT orbital configuration, cirrus occurrence is tied to convective processes triggered by solar radiation (Sassen et al. 2009). TOMCAT observations enable the derivation of diurnally consistent ice scattering models that benefit a host of operational and applied research endeavors, including more accurate radiative transfer for weather/climate models and improved remote sensing retrievals of ice cloud properties. Estimates of ice cloud diurnal variability and processes can be further enhanced by flying the TOMCAT sensors in orbit with a radar capable of measuring cloud properties.
- *Aerosols*: TOMCAT, like CATS before it, has robust nighttime 1,064 nm data to reliably detect the full vertical extent of aerosol plumes (Rajapakshe et al. 2017). In the daytime, the stereo camera imaging technique and AOCH retrieval from O_2 B band provides complementary information about smoke and dust injection heights across a wider swath over both source and downwind regions. Additionally, the two TOMCAT stereo imaging techniques can retrieve motion corresponding to the winds at the top of the plume. These capabilities, in combination with the TOMCAT orbital characteristics, enable the 3D characterization of smoke and dust at different times of day (Lee et al. 2019; Yu et al. 2020) that better constrain aerosol emissions, improve PBL and injection parameterization schemes in global models, and link emissions to downwind long-range transport patterns (Yu et al. 2019).
- *PBL*: While lidar-based AMLH is not identical to the thermodynamically defined PBLH, profiles of backscatter and extinction have been used widely for PBL and air quality process studies and in modern Earth system models that include aerosol emission, transport, and removal processes (Yu et al. 2012; Koffi et al. 2012; Yu et al. 2015; Liu et al. 2020). Together with surface-based PBL observations, TOMCAT's L3 data products describing the diurnal variation of aerosol extinction profiles and AMLH on regional and seasonal scales provide a dataset for 1) investigating PBL processes (science objective 2), complementing a future PBL-based satellite mission (Teixeira et al. 2021), and 3) advancing PBL parameterizations in weather, air quality, and climate models.

Validation and synergy. The vertical information from TOMCAT has strong synergy with ground-based networks and the next generation of geostationary atmospheric composition and weather satellites, and their coincident observations provide unprecedented three-dimensional (3D) time-varying observations of aerosol and cloud distributions. To estimate possible biases in the diurnal statistics due to seasonal or annual variability, data derived from surface sensing networks such as the Aerosol Robotic Network (AERONET; Holben et al. 1998), Micro-Pulse Lidar Network (MPLNET; Campbell et al. 2002), and ceilometer networks (Caicedo et al. 2020) can be used to evaluate and improve space-based data products. The estimates of aerosol and cloud diurnal variability from TOMCAT data are highly relevant to passive cloud and aerosol sensors in the program of record. The emergent constellation of GEO sensors for atmospheric composition, such as the Tropospheric Emissions: Monitoring Pollution (TEMPO) mission (Zoogman et al. 2009) and GEMS (Kim et al. 2019), as well as sun-synchronous sensors such as the Multi-Angle Imager for Aerosols (MAIA; Diner et al. 2018), will generate AOCH products. However, none of these passive sensors are equipped with an active lidar to accurately evaluate their AOCH products. TOMCAT data can be used to estimate biases in height retrievals from next generation GEO sensors due to solar zenith angle, limb angle, and scattering angle. TOMCAT also has strong synergy with the current generation of GEO weather satellites, such as Geostationary Operational Environmental Satellite (*GOES-16*/*-17*) Advanced Baseline Imager (ABI; Schmit et al. 2016). Ice cloud data products (i.e., cloud fraction, effective radius, cloud-top height, etc.) and aerosol products (i.e., AOD) from ABI and other GEO weather satellites complement TOMCAT data products. At night, TOMCAT lidar data may also be combined with the infrared bands from GEO imagers to improve the retrievals of dust-layer height and cloud-top height, reducing the uncertainties that otherwise could be large due to errors in surface temperature and atmospheric profile of temperature and water vapor.

Applications. TOMCAT NRT data products enable timely and precise monitoring of the height and vertical distribution of aerosols and support two applications objectives (Fig. 5) that uniquely assist operational hazardous plume monitoring, aerosol modeling, and air quality forecasts. TOMCAT data are transmitted, received, processed, and distributed to application end users with the <4 h latency needed for incorporation into operational center forecasting systems (Benedetti et al. 2018). TOMCAT excels at differentiating free troposphere from boundary layer aerosol events, leading to the development of better attribution of column aerosol loading in the vertical that improves aerosol monitoring and related decision support along major air routes between Asia, North America, and Europe. The TOMCAT NRT aerosol profiles and injection heights provide information about the vertical structure of hazardous plumes and directly address critical data needs identified by forecasting agencies. At night

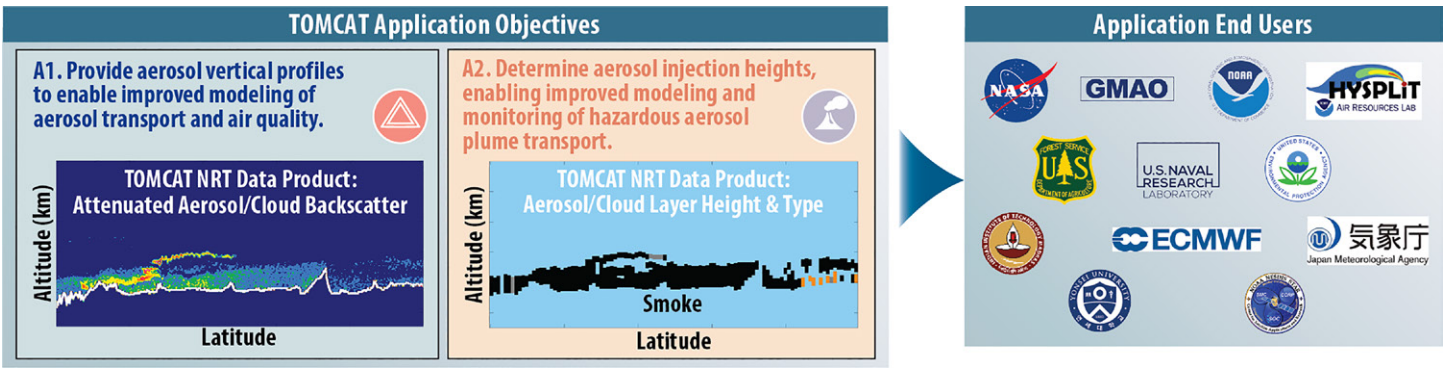

Fig. 5. TOMCAT would achieve (left) two application objectives through its ability to provide NRT data to (right) application end users within 4 h and point off-nadir 20° with pointing accuracy of 200 m to sample hazardous events.

when the TOMCAT imager is not available to provide supplementary aerosol-layer information, the TOMCAT lidar, via its 20° (equivalent to 160 km for an orbit altitude of 435 km) off-nadir-pointing capability, may be directed to point to an area of interest (or during the day) to increase the frequency of profiling of the hazardous plumes. Several studies have outlined methods of including lidar detections of ash from CATS or CALIOP into an operational ash modeling framework (Vernier et al. 2013; Prata et al. 2015; Hughes et al. 2016). This type of data is also invaluable for verification of model output (Dacre et al. 2015; Crawford et al. 2016) as well as insight into mixing processes of the downwind volcanic ash cloud layers (Bursik et al. 2021). Rerouting air traffic around volcanic ash requires an operational forecast of hazardous regions produced by Volcanic Ash Advisory Centers (VAACs) worldwide. The need for precise information on the vertical structure of volcanic ash clouds has never been greater, as the International Airways Volcano Watch (IAVW), which defines VAAC products and services, is evolving to include quantitative ash concentration forecasts (IAVW; WMO 2020). Similarly, the National Wildfire Coordinating Group (NWCG; Lindley et al. 2020) recommends the need to "support the development of satellite missions and products that provide information about the vertical structure of smoke and aerosols" and "advocate for the inclusion of LIDARs, and/or the development of other technologies capable of direct sampling or derivation of smoke height, onboard future spacecraft." TOMCAT NRT data products provide significant societal and economic benefits by meeting both the VAAC and NWCG needs.

Concluding remarks, significance, and summary

As stated in the 2017–27 Decadal Survey for Earth Science and Applications from Space, "Global, or near-global coverage of pollutants (e.g., PM, O_3, and NO_2) with diurnal variation is important to link air quality to health and ecosystem damages and to identify source impacts on air quality." While several current (i.e., GEMS) and upcoming (i.e., TEMPO) missions provide coverage of the northern midlatitudes, these missions provide limited vertical information and do not cover much of central Asia, Africa, and the tropics where population growth and poor air quality are expected. It is critical to measure the spatiotemporal evolution of aerosols over these regions in the coming decades from space. The timing is perfect, as the past two decades have seen the rapid growth of revolutionary and emerging new technologies for Earth observation, enabling smaller and more affordable sensors that fly on multiple SmallSats to better observe the spatiotemporal variability and processes of clouds and aerosols not observed from the NASA EOS and/or GEO sensors.

In this paper, we outline a SmallSat mission concept that provides time-varying optical measurements of cloud and aerosol transport called TOMCAT. This mission concept couples active (lidar) and passive (imager) remote sensing observations to provide measurements of vertical profiles of backscatter and depolarization ratio required to retrieve cloud and aerosol physical parameters (Fig. 2), as well as multiangle radiance in the visible spectrum to determine cloud and aerosol plume heights. The TOMCAT mission concept 1) addresses the gaps in our understanding of aerosol, cloud, and PBLH spatiotemporal variability, 2) embraces the technology advances in smaller sensors and spacecraft, 3) leverages the heritage of the CATS and MISR measurement capabilities, 4) provides timely and precise monitoring of the height and vertical distribution of aerosols to improve air quality and hazardous plume transport predictions, and 5) offers an affordable option (<$200 million complete, full lifetime mission cost) that is ~5–6 times less than the typical flagship missions.

While we present one mission concept in this paper (a single spacecraft version), the SmallSat lidar enables many types of mission concepts besides TOMCAT. For example, four copies of the TOMCAT concept in the same orbital plane with spacecraft 90° apart (~6 h) would further improve the temporal sampling and ability to statistically resolve the diurnal variability of clouds and aerosols ("TOMCAT provides unprecedented sampling to

statistically resolve diurnal variability at nearly global scale" sidebar). The Earth science community should leverage the evolution of affordable spacecraft buses and rideshare launches over the coming decades by designing missions that utilize a distributed architecture of SmallSats and CubeSats to achieve unprecedented spatiotemporal sampling.

Acknowledgments. In addition to the authors of this paper, the following people contributed to the TOMCAT simulations and algorithm plans: Stephen Nicholls, James Limbacher, and Patrick Selmer from Science Systems and Applications, Inc. (SSAI). We also thank Xi Chen for contributions to Fig. 4 and the in-kind support from University of Iowa for his participation in TOMCAT mission planning. Also, a special thanks to the following scientists that have identified themselves as potential data users for the TOMCAT applications during the concept development: Arlindo Da Silva, Virginie Buchard, and Nickolay Krotkov from NASA GSFC; Juli Rubin from NRL; Ariel Stein from NOAA ARL; K. Wyat Appel from the U.S. Environmental Protection Agency; Jamie Kibler and Jeffrey Osiensky from the Volcanic Ash Advisory Center (Washington, D.C., and Anchorage, Alaska, respectively); Jeff McQueen from NOAA National Center for Environmental Prediction; Yi Ming from NOAA Geophysical Fluid Dynamics Laboratory; Susan O'Neill from the USDA Forest Services; Taichu Tanaka from the Meteorological Research Institute at the Japan Meteorological Agency (Japan); and Sachin Ghude from the Indian Institute of Tropical Meteorology (India). Finally, we thank the NASA Earth Science Technology Office (ESTO) for providing funding for technology development relevant to the TOMCAT concept.

Data availability statement. The data used in this paper to demonstrate the TOMCAT lidar and imager data come from the CATS, VIIRS, MISR, and TROPOMI missions. The data from these missions are freely available at the links below:

- CATS: https://eosweb.larc.nasa.gov/project/CATS-ISS
- VIIRS: www.earthdata.nasa.gov/learn/find-data/near-real-time/viirs
- MISR: https://eosweb.larc.nasa.gov/project/MISR
- TROPOMI: www.tropomi.eu/data-products/data-access

Data from the GEOS Nature Run using in the "TOMCAT provides unprecedented sampling to statistically resolve diurnal variability at nearly global scale" sidebar sampling study can be accessed here: https://gmao.gsfc.nasa.gov/global_mesoscale/7km-G5NR/data_access/.

References

Andela, N., J. W. Kaiser, G. R. van der Werf, and M. J. Wooster, 2015: New fire diurnal cycle characterizations to improve fire radiative energy assessments made from MODIS observations. *Atmos. Chem. Phys.*, **15**, 8831–8846, https://doi.org/10.5194/acp-15-8831-2015.

Baklanov, A., and Coauthors, 2017: Key issues for seamless integrated chemistry–meteorology modeling. *Bull. Amer. Meteor. Soc.*, **98**, 2285–2292, https://doi.org/10.1175/BAMS-D-15-00166.1.

Benedetti, A., and Coauthors, 2018: Status and future of numerical atmospheric aerosol prediction with a focus on data requirements. *Atmos. Chem. Phys.*, **18**, 10 615–10 643, https://doi.org/10.5194/acp-18-10615-2018.

Blackwell, W. J., and Coauthors, 2018: An overview of the TROPICS NASA Earth Venture Mission. *Quart. J. Roy. Meteor. Soc.*, **144**, 16–26, https://doi.org/10.1002/qj.3290.

Bursik, M., Q. Y. Yang, A. Bear-Crozier, M. Pavolonis, and A. Tupper, 2021: The development of volcanic ash cloud layers over hours to days due to atmospheric turbulence layering. *Atmosphere*, **12**, 285, https://doi.org/10.3390/atmos12020285.

Caicedo, V., R. Delgado, R. Sakai, T. Knepp, D. Williams, K. Cavender, B. Lefer, and J. Szykman, 2020: An automated common algorithm for planetary boundary layer retrievals using aerosol lidars in support of the U.S. EPA Photochemical Assessment Monitoring Stations program. *J. Atmos. Oceanic Technol.*, **37**, 1847–1864, https://doi.org/10.1175/JTECH-D-20-0050.1.

Campbell, J. R., D. L. Hlavka, E. J. Welton, C. J. Flynn, D. D. Turner, J. D. Spinhirne, V. S. Scott III, and I. H. Hwang, 2002: Full-time, eye-safe cloud and aerosol lidar observation at Atmospheric Radiation Measurement program sites: Instruments and data processing. *J. Atmos. Oceanic Technol.*, **19**, 431–442, https://doi.org/10.1175/1520-0426(2002)019<0431:FTESCA>2.0.CO;2.

——, S. Lolli, J. R. Lewis, Y. Gu, and E. J. Welton, 2016: Daytime cirrus cloud top-of-the-atmosphere radiative forcing properties at a midlatitude site and their global consequences. *J. Appl. Meteor. Climatol.*, **55**, 1667–1679, https://doi.org/10.1175/JAMC-D-15-0217.1.

Carr, J. L., D. L. Wu, M. A. Kelly, and J. Gong, 2018: MISR-GOES 3D winds: Implications for future LEO-GEO and LEO-LEO winds. *Remote Sens.*, **10**, 1885, https://doi.org/10.3390/rs10121885.

——, ——, R. E. Wolfe, H. Madani, G. Lin, and B. Tan, 2019: Joint 3D-wind retrievals with stereoscopic views from MODIS and GOES. *Remote Sens.*, **11**, 2100, https://doi.org/10.3390/rs11182100.

Chen, X., and Coauthors, 2021: First retrieval of absorbing aerosol height over dark target using TROPOMI oxygen B band: Algorithm development and application for surface particulate matter estimates. *Remote Sens. Environ.*, **265**, 112674, https://doi.org/10.1016/j.rse.2021.112674.

Crawford, A. M., B. J. B. Stunder, F. Ngan, and M. J. Pavolonis, 2016: Initializing HYSPLIT with satellite observations of volcanic ash: A case study of the 2008 Kasatochi eruption. *J. Geophys. Res. Atmos.*, **121**, 10 786–10 803, https://doi.org/10.1002/2016JD024779.

Dacre, H. F., A. L. M. Grant, N. J. Harvey, D. J. Thomson, H. N. Webster, and F. Marenco, 2015: Volcanic ash layer depth: Processes and mechanisms. *Geophys. Res. Lett.*, **42**, 637–645, https://doi.org/10.1002/2014GL062454.

Dang, R. J., Y. Yang, X. M. Hu, Z. T. Wang, and S. W. Zhang, 2019: A review of techniques for diagnosing the atmospheric boundary layer height (ABLH) using aerosol lidar data. *Remote Sens.*, **11**, 1590, https://doi.org/10.3390/rs11131590.

Delgado-Bonal, A., A. Marshak, Y. Yang, and L. Oreopoulos, 2022: Cloud height daytime variability from DSCOVR/EPIC and GOES-R/ABI observations. *Front. Remote Sens.*, **3**, 780243, https://doi.org/10.3389/frsen.2022.780243.

Diner, D. J., and Coauthors, 1998: Multi-angle Imaging Spectroradiometer (MISR) instrument description and experiment overview. *IEEE Trans. Geosci. Remote Sens.*, **36**, 1072–1087, https://doi.org/10.1109/36.700992.

——, and Coauthors, 2018: Advances in multiangle satellite remote sensing of speciated airborne particulate matter and association with adverse health effects: From MISR to MAIA. *J. Appl. Remote Sens.*, **12**, 042603, https://doi.org/10.1117/1.JRS.12.042603.

El Amraoui, L., B. Sic, A. Piacentini, V. Marecal, N. Frebourg, and J. L. Attie, 2020: Aerosol data assimilation in the MOCAGE chemical transport model during the TRAQA/ChArMEx campaign: Lidar observations. *Atmos. Meas. Tech.*, **13**, 4645–4667, https://doi.org/10.5194/amt-13-4645-2020.

Eresmaa, N., A. Karppinen, S. M. Joffre, J. Räsänen, and H. Talvitie, 2006: Mixing height determination by ceilometer. *Atmos. Chem. Phys.*, **6**, 1485–1493, https://doi.org/10.5194/acp-6-1485-2006.

Esau, I., and S. Zilitinkevich, 2010: On the role of the planetary boundary layer depth in the climate system. *Adv. Sci. Res.*, **4**, 63–69, https://doi.org/10.5194/asr-4-63-2010.

Escribano, J., and Coauthors, 2022: Assimilating spaceborne lidar dust extinction can improve dust forecasts. *Atmos. Chem. Phys.*, **22**, 535–560, https://doi.org/10.5194/acp-22-535-2022.

Getzewich, B. J., and Coauthors, 2018: CALIPSO lidar calibration at 532 nm: Version 4 daytime algorithm. *Atmos. Meas. Tech.*, **11**, 6309–6326, https://doi.org/10.5194/amt-11-6309-2018.

Giglio, L., 2007: Characterization of the tropical diurnal fire cycle using VIRS and MODIS observations. *Remote Sens. Environ.*, **108**, 407–421, https://doi.org/10.1016/j.rse.2006.11.018.

Heymsfield, A. J., D. Winker, M. Avery, M. Vaughan, G. Diskin, M. Deng, V. Mitev, and R. Matthey 2014: Relationships between ice water content and volume extinction coefficient from in situ observations for temperatures from 0° to −86°C: Implications for spaceborne lidar retrievals. *J. Appl. Meteor. Climatol.*, **53**, 479–505, https://doi.org/10.1175/JAMC-D-13-087.1.

Hlavka, D. L., J. E. Yorks, S. A. Young, M. A. Vaughan, R. E. Kuehn, M. J. McGill, and S. D. Rodier, 2012: Airborne validation of cirrus cloud properties derived from CALIPSO lidar measurements: Optical properties. *J. Geophys. Res.*, **117**, D09207, https://doi.org/10.1029/2011JD017053.

Holben, B. N., and Coauthors, 1998: AERONET—A federated instrument network and data archive for aerosol characterization. *Remote Sens. Environ.*, **66**, 1–16, https://doi.org/10.1016/S0034-4257(98)00031-5.

Holtslag, A. A. M., and Coauthors, 2013: Stable atmospheric boundary layers and diurnal cycles: Challenges for weather and climate models. *Bull. Amer. Meteor. Soc.*, **94**, 1691–1706, https://doi.org/10.1175/BAMS-D-11-00187.1.

Horváth, A., and R. Davies, 2001: Feasibility and error analysis of cloud motion wind extraction from near-simultaneous multiangle MISR measurements. *J. Atmos. Oceanic Technol.*, **18**, 591–608, https://doi.org/10.1175/1520-0426(2001)018<0591:FAEAOC>2.0.CO;2.

Hou, A. Y., and Coauthors, 2014: The Global Precipitation Measurement mission. *Bull. Amer. Meteor. Soc.*, **95**, 701–722, https://doi.org/10.1175/BAMS-D-13-00164.1.

Huff, A., S. Kondragunta, H. Zhang, I. Laszlo, M. Zhou, V. Caicedo, R. Delgado, and R. Levy, 2021: Tracking smoke from a prescribed fire and its impacts on local air quality using temporally resolved *GOES-16* ABI aerosol optical depth (AOD). *J. Atmos. Oceanic Technol.*, **38**, 963–976, https://doi.org/10.1175/JTECH-D-20-0162.1.

Hughes, E. J., J. Yorks, N. A. Krotkov, A. M. da Silva, and M. McGill, 2016: Using CATS near-real-time lidar observations to monitor and constrain volcanic sulfur dioxide (SO_2) forecasts. *Geophys. Res. Lett.*, **43**, 11 089–11 097, https://doi.org/10.1002/2016GL070119.

Kar, J., and Coauthors, 2018: CALIPSO lidar calibration at 532 nm: Version 4 nighttime algorithm. *Atmos. Meas. Tech.*, **11**, 1459–1479, https://doi.org/10.5194/amt-11-1459-2018.

Kim, J., and Coauthors, 2019: New era of air quality monitoring from space: Geostationary Environment Monitoring Spectrometer (GEMS). *Bull. Amer. Meteor. Soc.*, **101**, E1–E22, https://doi.org/10.1175/BAMS-D-18-0013.1.

King, M. D., S. Platnick, W. P. Menzel, S. A. Ackerman, and P. A. Hubanks, 2013: Spatial and temporal distribution of clouds observed by MODIS onboard the Terra and Aqua satellites. *IEEE Trans. Geosci. Remote Sens.*, **51**, 3826–3852, https://doi.org/10.1109/TGRS.2012.2227333.

Kipling, Z., and Coauthors, 2016: What controls the vertical distribution of aerosol? Relationships between process sensitivity in HadGEM3–UKCA and inter-model variation from AeroCom phase II. *Atmos. Chem. Phys.*, **16**, 2221–2241, https://doi.org/10.5194/acp-16-2221-2016.

Koffi, B., and Coauthors, 2012: Application of the CALIOP layer product to evaluate the vertical distribution of aerosols estimated by global models: AeroCom phase I results. *J. Geophys. Res.*, **117**, D10201, https://doi.org/10.1029/2011JD016858.

Kondragunta, S., H. Zhang, P. Ciren, I. Laszlo, and D. Tong, 2018: Tracking dust storms using the latest satellite technology: The Rapid Refresh GOES-16 Advanced Baseline Imager. *EM Magazine*, May, A&WMA, Pittsburgh, PA, https://airandwmapa.sharepoint.com/sites/AWMA_Website/Shared%20Documents/Forms/AllItems.aspx?id=%2Fsites%2FAWMA%5FWebsite%2FShared%20Documents%2Fem%2Ddo%20not%20delete%2F2018%2F5%2Fkondragunta%2Epdf&parent=%2Fsites%2FAWMA%5FWebsite%2FShared%20Documents%2Fem%2Ddo%20not%20delete%2F2018%2F5&p=true&ga=1.

Lee, L., J. Zhang, J. S. Reid, and J. E. Yorks, 2019: Investigation of CATS aerosol products and application toward global diurnal variation of aerosols. *Atmos. Chem. Phys.*, **19**, 12 687–12 707, https://doi.org/10.5194/acp-19-12687-2019.

Lelieveld, J., J. S. Evans, M. Fnais, D. Giannadaki, and A. Pozzer, 2015: The contribution of outdoor air pollution sources to premature mortality on a global scale. *Nature*, **525**, 367–371, https://doi.org/10.1038/nature15371.

Li, Z., and Coauthors, 2017: Aerosol and boundary-layer interactions and impact on air quality. *Natl. Sci. Rev.*, **4**, 810–833, https://doi.org/10.1093/nsr/nwx117.

Lindley, T. T., and Coauthors, 2020: Report on satellite technology requirements for wildland fire services in the CONUS. NWCGS Satellite Data Task Team Rep., 35 pp., www.nwcg.gov/sites/default/files/committee/docs/fenc-satellite-data-task-team-final-report.pdf.

Liu, C., M. Gao, Q. Hu, G. P. Brasseur, and G. R. Carmichael, 2020: Stereoscopic monitoring: A promising strategy to advance diagnostic and prediction of air pollution. *Bull. Amer. Meteor. Soc.*, **102**, E730–E737, https://doi.org/10.1175/BAMS-D-20-0217.1.

Liu, S., and X.-Z. Liang, 2010: Observed diurnal cycle climatology of planetary boundary layer height. *J. Climate*, **23**, 5790–5809, https://doi.org/10.1175/2010JCLI3552.1.

Mace, G. G., Q. Zhang, M. Vaughan, R. Marchand, G. Stephens, C. Trepte, and D. Winker, 2009: A description of hydrometeor layer occurrence statistics derived from the first year of merged CloudSat and CALIPSO data. *J. Geophys. Res.*, **114**, D00A26, https://doi.org/10.1029/2007JD009755.

Malin, M. C., and Coauthors, 2010: An overview of the 1985–2006 Mars Orbiter Camera science investigation. *Mars*, **5**, 1–60, https://doi.org/10.1555/mars.2010.0001.

Markus, T., and Coauthors, 2017: The Ice, Cloud, and Land Elevation Satellite-2 (ICESat-2): Science requirements, concept, and implementation. *Remote Sens. Environ.*, **190**, 260–273, https://doi.org/10.1016/j.rse.2016.12.029.

McGill, M., D. Hlavka, W. Hart, V. S. Scott, J. Spinhirne, and B. Schmid, 2002: Cloud physics lidar: Instrument description and initial measurement results. *Appl. Opt.*, **41**, 3725–3734, https://doi.org/10.1364/AO.41.003725.

——, M. A. Vaughan, C. R. Trepte, W. D. Hart, D. L. Hlavka, D. M. Winker, and R. Kuehn, 2007: Airborne validation of spatial properties measured by the CALIPSO lidar. *J. Geophys. Res.*, **112**, D20201, https://doi.org/10.1029/2007JD008768.

——, J. E. Yorks, V. S. Scott, A. W. Kupchock, and P. A. Selmer, 2015: The Cloud-Aerosol Transport System (CATS): A technology demonstration on the International Space Station. *Proc. SPIE*, **9612**, 96120A, https://doi.org/10.1117/12.2190841.

McGrath-Spangler, E. L., and A. S. Denning, 2013: Global seasonal variations of midday planetary boundary layer depth from CALIPSO space-borne lidar. *J. Geophys. Res. Atmos.*, **118**, 1226–1233, https://doi.org/10.1002/jgrd.50198.

Miller, S., C. C. Schmidt, T. J. Schmit, and D. W. Hillger, 2012: A case for natural colour imagery from geostationary satellites, and an approximation for the GOES-R ABI. *Int. J. Remote Sens.*, **33**, 3999–4028, https://doi.org/10.1080/01431161.2011.637529.

Molod, A., H. Salmun, and A. B. Marquardt Collow, 2019: Annual cycle of planetary boundary layer heights estimated from wind profiler network data. *J. Geophys. Res. Atmos.*, **124**, 6207–6221, https://doi.org/10.1029/2018JD030102.

Mueller, K. J., and Coauthors, 2017: Assessment of MISR cloud motion vectors (CMVs) relative to GOES and MODIS atmospheric motion vectors (AMVs). *J. Appl. Meteor. Climatol.*, **56**, 555–572, https://doi.org/10.1175/JAMC-D-16-0112.1.

Murray, C. J. L., and Coauthors, 2020: Global burden of 87 risk factors in 204 countries and territories, 1990–2019: A systematic analysis for the Global Burden of Disease Study 2019. *Lancet*, **396**, 1223–1249, https://doi.org/10.1016/S0140-6736(20)30752-2.

Nanda, S., M. De Graaf, J. P. Veefkind, M. Ter Linden, M. Sneep, J. De Haan, and P. F. Levelt, 2019: A neural network radiative transfer model approach applied to the Tropospheric Monitoring Instrument aerosol height algorithm. *Atmos. Meas. Tech.*, **12**, 6619–6634, https://doi.org/10.5194/amt-12-6619-2019.

National Academies of Sciences, Engineering, and Medicine, 2018: *Thriving on Our Changing Planet: A Decadal Strategy for Earth Observation from Space.* National Academies Press, 700 pp.

Nelson, D. L., M. J. Garay, R. A. Kahn, and B. A. Dunst, 2013: Stereoscopic height and wind retrievals for aerosol plumes with the MISR Interactive Explorer (MINX). *Remote Sens.*, **5**, 4593–4628, https://doi.org/10.3390/rs5094593.

Noel, V., H. Chepfer, M. Chiriaco, and J. Yorks, 2018: The diurnal cycle of cloud profiles over land and ocean between 51°S and 51°N, seen by the CATS spaceborne lidar from the International Space Station. *Atmos. Chem. Phys.*, **18**, 9457–9473, https://doi.org/10.5194/acp-18-9457-2018.

Nowottnick, E., and Coauthors, 2022: Aerosol detection from the cloud aerosol transport system on the International Space Station: Algorithm overview and implications for diurnal sampling. *Atmosphere*, **13**, 1439, https://doi.org/10.3390/atmos13091439.

Omar, A. H., and Coauthors, 2009: The *CALIPSO* automated aerosol classification and lidar ratio selection algorithm. *J. Atmos. Oceanic Technol.*, **26**, 1994–2014, https://doi.org/10.1175/2009JTECHA1231.1.

Painemal, D., P. Minnis, and L. O'Neill, 2013: The diurnal cycle of cloud-top height and cloud cover over the southeastern Pacific as observed by *GOES-10*. *J. Atmos. Sci.*, **70**, 2393–2408, https://doi.org/10.1175/JAS-D-12-0325.1.

Palm, S. P., P. A. Selmer, J. E. Yorks, S. Nicholls, and E. P. Nowottnick, 2021: Planetary boundary layer height estimates from ICESat-2 and CATS backscatter measurements. *Frontiers*, **2**, 716951, https://doi.org/10.3389/frsen.2021.716951.

Patnaude, R., M. Diao, X. Liu, and S. Chu, 2021: Effects of thermodynamics, dynamics and aerosols on cirrus clouds based on in situ observations and NCAR CAM6 model. *Atmos. Phys. Chem.*, **21**, 1835–1859, https://doi.org/10.5194/acp-21-1835-2021.

Pauly, R. M., and Coauthors, 2019: Cloud-Aerosol Transport System (CATS) 1064 nm calibration and validation. *Atmos. Meas. Tech.*, **12**, 6241–6258, https://doi.org/10.5194/amt-12-6241-2019.

Peral, E., and Coauthors, 2019: RainCube: The first ever radar measurements from a CubeSat in space. *J. Appl. Remote Sens.*, **13**, 032504, https://doi.org/10.1117/1.JRS.13.032504.

Prata, A. T., S. T. Siems, and M. J. Manton, 2015: Quantification of volcanic cloud top heights and thicknesses using A-train observations for the 2008 Chaiten eruption. *J. Geophys. Res. Atmos.*, **120**, 2928–2950, https://doi.org/10.1002/2014JD022399.

Rajapakshe, C., Z. Zhang, J. E. Yorks, H. Yu, Q. Tan, K. Meyer, and S. Platnick, 2017: Seasonally transported aerosol layers over southeast Atlantic are closer to underlying clouds than previously reported. *Geophys. Res. Lett.*, **44**, 5818–5825, https://doi.org/10.1002/2017GL073559.

Reising, S. C., and Coauthors, 2016: Temporal Experiment for Storms and Tropical Systems Technology Demonstration (TEMPEST-D): Reducing risk for 6U-class

nanosatellite constellations. *2016 IEEE International Geoscience and Remote Sensing Symp.*, Beijing, China, IEEE, 5559–5560, https://doi.org/10.1109/IGARSS.2016.7730451.

Sassen, K., Z. Wang, and D. Liu, 2009: Cirrus clouds and deep convection in the tropics: Insights from CALIPSO and CloudSat. *J. Geophys. Res.*, **114**, D00H06, https://doi.org/10.1029/2009JD011916.

Schmit, T. J., P. Griffith, M. M. Gunshor, J. M. Daniels, S. J. Goodman, and W. J. Lebair, 2016: A closer look at the ABI on the GOES-R series. *Bull. Amer. Meteor. Soc.*, **98**, 681–698, https://doi.org/10.1175/BAMS-D-15-00230.1.

Seibert, P., F. Beyrich, S.-E. Gryning, S. Joffre, A. Rasmussen, and P. Tercier, 2000: Review and intercomparison of operational methods for the determination of the mixing height. *Atmos. Environ.*, **34**, 1001–1027, https://doi.org/10.1016/S1352-2310(99)00349-0.

Seidel, D. J., C. O. Ao, and K. Li, 2010: Estimating climatological planetary boundary layer heights from radiosonde observations: Comparison of methods and uncertainty analysis. *J. Geophys. Res.*, **115**, D16113, https://doi.org/10.1029/2009JD013680.

——, Y. Zhang, A. Beljaars, J.-C. Golaz, A. R. Jacobson, and B. Medeiros, 2012: Climatology of the planetary boundary layer over the continental United States and Europe. *J. Geophys. Res.*, **117**, D17106, https://doi.org/10.1029/2012JD018143.

Sekiyama, T. T., T. Y. Tanaka, A. Shimizu, and T. Miyoshi, 2010: Data assimilation of CALIPSO aerosol observations. *Atmos. Chem. Phys.*, **10**, 39–49, https://doi.org/10.5194/acp-10-39-2010.

Selva, D., and D. Krejci, 2012: A survey and assessment of the capabilities of CubeSats for Earth observation. *Acta Astronaut.*, **74**, 50–68, https://doi.org/10.1016/j.actaastro.2011.12.014.

Shin, H. H., Y. Ming, M. Zhao, J.-C. Golaz, B. Xiang, and H. Guo, 2018: Evaluation of planetary boundary layer simulation in GFDL atmospheric general circulation models. *J. Climate*, **31**, 5071–5087, https://doi.org/10.1175/JCLI-D-17-0543.1.

Stephens, G. L., and Coauthors, 2003: The *CloudSat* mission and the A-train: A new dimension of space-based observations of clouds and precipitation. *Bull. Amer. Meteor. Soc.*, **83**, 1771–1790, https://doi.org/10.1175/BAMS-83-12-1771.

——, and Coauthors, 2020: The emerging technological revolution in Earth observations. *Bull. Amer. Meteor. Soc.*, **101**, E274–E285, https://doi.org/10.1175/BAMS-D-19-0146.1.

Teixeira, J., and Coauthors, 2021: Toward a global planetary boundary layer observing system. NASA PBL Incubation Study Team Rep., 134 pp., https://science.nasa.gov/science-red/s3fs-public/atoms/files/NASAPBLIncubationFinalReport.pdf.

Uno, I., and Coauthors, 2009: Asian dust transported one full circuit around the globe. *Nat. Geosci.*, **2**, 557–560, https://doi.org/10.1038/ngeo583.

Vaughan, M., and Coauthors, 2009: Fully automated detection of cloud and aerosol layers in the *CALIPSO* lidar measurements. *J. Atmos. Oceanic Technol.*, **26**, 2034–2050, https://doi.org/10.1175/2009JTECHA1228.1.

——, and Coauthors, 2019: CALIPSO lidar calibration at 1064 nm: Version 4 algorithm. *Atmos. Meas. Tech.*, **12**, 51–82, https://doi.org/10.5194/amt-12-51-2019.

Vernier, J. P., and Coauthors, 2013: An advanced system to monitor the 3D structure of diffuse volcanic ash clouds. *J. Appl. Meteor. Climatol.*, **52**, 2125–2138, https://doi.org/10.1175/JAMC-D-12-0279.1.

Vignesh, P. P., J. H. Jiang, P. Kishore, H. Su, T. Smay, N. Brighton, and I. Velicogna, 2020: Assessment of CMIP6 cloud fraction and comparison with satellite observations. *Earth Space Sci.*, **7**, e2019EA000975, https://doi.org/10.1029/2019EA000975.

Wang, J., and S. A. Christopher, 2006: Mesoscale modeling of Central American smoke transport to the United States: 2. Smoke radiative impact on regional surface energy budget and boundary layer evolution. *J. Geophys. Res.*, **111**, D14S92, https://doi.org/10.1029/2005JD006720.

——, and Coauthors, 2003: GOES 8 retrieval of dust aerosol optical thickness over the Atlantic Ocean during PRIDE. *J. Geophys. Res.*, **108**, 8595, https://doi.org/10.1029/2002JD002494.

——, X. Xia, P. Wang, and S. A. Christopher, 2004: Diurnal variability of dust aerosol optical thickness and angstrom exponent over dust source regions in China. *Geophys. Res. Lett.*, **31**, L08107, https://doi.org/10.1029/2004GL019580.

——, S. A. Christopher, U. S. Nair, J. S. Reid, E. M. Prins, J. Szykman, and J. L. Hand, 2006: Mesoscale modeling of Central American smoke transport to the United States, 1: "Top-down" assessment of emission strength and diurnal variation impacts. *J. Geophys. Res.*, **111**, D05S17, https://doi.org/10.1029/2005JD006416.

Winker, D. M., M. A. Vaughan, A. Omar, Y. Hu, K. A. Powell, Z. Liu, W. H. Hunt, and S. A. Young, 2009: Overview of the *CALIPSO* mission and CALIOP data processing algorithms. *J. Atmos. Oceanic Technol.*, **26**, 2310–2323, https://doi.org/10.1175/2009JTECHA1281.1.

WMO, 2020: Meteorological satellite product development in support of the International Airways Volcano Watch. WMO Working Paper 5, 12 pp.

Wu, D. L., and Coauthors, 2009: Vertical distributions and relationships of cloud occurrence frequency as observed by MISR, AIRS, MODIS, OMI, CALIPSO, and CloudSat. *Geophys. Res. Lett.*, **36**, L09821, https://doi.org/10.1029/2009GL037464.

Xian, P., and Coauthors, 2019: Current state of the global operational aerosol multi-model ensemble: An update from the International Cooperative for Aerosol Prediction (ICAP). *Quart. J. Roy. Meteor. Soc.*, **145**, 176–209, https://doi.org/10.1002/qj.3497.

Xu, X., and Coauthors, 2017: Passive remote sensing of altitude and optical depth of dust plumes using the oxygen A and B bands: First results from EPIC/DSCOVR at Lagrange-1 point. *Geophys. Res. Lett.*, **44**, 7544–7554, https://doi.org/10.1002/2017GL073939.

——, J. Wang, Y. Wang, and A. Kokhanovsky, 2018: Passive remote sensing of aerosol height. *Remote Sensing of Aerosols, Clouds, and Precipitation*, T. Islam et al., Eds., Elsevier, 1–22.

——, and Coauthors, 2019: Detecting layer height of smoke aerosols over vegetated land and water surfaces via oxygen absorption bands: Hourly results from EPIC/DSCOVR in deep space. *Atmos. Meas. Tech.*, **12**, 3269–3288, https://doi.org/10.5194/amt-12-3269-2019.

Yang, D., C. Li, A. K.-H. Lau, and Y. Li, 2013: Long-term measurement of daytime atmospheric mixing layer height over Hong Kong. *J. Geophys. Res. Atmos.*, **118**, 2422–2433, https://doi.org/10.1002/jgrd.50251.

Ye, H. C., and Coauthors, 2021: Impact of CALIPSO profile data assimilation on 3-D aerosol improvement in a size-resolved aerosol model. *Atmos. Res.*, **264**, 105877, https://doi.org/10.1016/j.atmosres.2021.105877.

Yin, J., and A. Porporato, 2017: Diurnal cloud cycle biases in climate models. *Nat. Commun.*, **8**, 2269, https://doi.org/10.1038/s41467-017-02369-4.

Yorks, J. E., and Coauthors, 2016: An overview of the CATS level 1 processing algorithms and data products. *Geophys. Res. Lett.*, **43**, 4632–4639, https://doi.org/10.1002/2016GL068006.

——, P. A. Selmer, A. Kupchock, E. P. Nowottnick, K. Christian, D. Rusinek, N. Dacic, and M. J. McGill, 2021: Aerosol and cloud detection using machine learning algorithms and space-based lidar data. *Atmosphere*, **12**, 606, https://doi.org/10.3390/atmos12050606.

Young, S. A., and M. A. Vaughan, 2009: The retrieval of profiles of particulate extinction from *Cloud-Aerosol Lidar Infrared Pathfinder Satellite Observations* (*CALIPSO*) data: Algorithm description. *J. Atmos. Oceanic Technol.*, **26**, 1105–1119, https://doi.org/10.1175/2008JTECHA1221.1.

Yu, H., L. A. Remer, M. Chin, H. Bian, Q. Tan, T. Yuan, and Y. Zhang, 2012: Aerosols from overseas rival domestic emissions over North America. *Science*, **337**, 566–569, https://doi.org/10.1126/science.1217576.

——, and Coauthors, 2015: Quantification of trans-Atlantic dust transport from seven-year (2007–2013) record of CALIPSO lidar measurements. *Remote Sens. Environ.*, **159**, 232–249, https://doi.org/10.1016/j.rse.2014.12.010.

——, and Coauthors, 2019: Estimates of African dust deposition along the trans-Atlantic transit using the decadelong record of aerosol measurements from CALIOP, MODIS, MISR, and IASI. *J. Geophys. Res. Atmos.*, **124**, 7975–7996, https://doi.org/10.1029/2019JD030574.

Yu, Y., and Coauthors, 2020: Disproving the Bodélé depression as the primary source of dust fertilizing the Amazon rainforest. *Geophys. Res. Lett.*, **47**, e2020GL088020, https://doi.org/10.1029/2020GL088020.

——, and Coauthors, 2021: A global analysis of diurnal variability in dust and dust mixture using CATS observations. *Atmos. Chem. Phys.*, **21**, 1427–1447, https://doi.org/10.5194/acp-21-1427-2021.

Zhang, J., J. R. Campbell, J. S. Reid, D. L. Westphal, N. L. Baker, W. F. Campbell, and E. J. Hyer, 2011: Evaluating the impact of assimilating CALIOP-derived aerosol extinction profiles on a global mass transport model. *Geophys. Res. Lett.*, **38**, L14801, https://doi.org/10.1029/2011GL047737.

Zhang, X., and S. Kondragunta, 2008: Temporal and spatial variability in biomass burned areas across the USA derived from the GOES fire product. *Remote Sens. Environ.*, **112**, 2886–2897, https://doi.org/10.1016/j.rse.2008.02.006.

Zhang, Y., K. Sun, Z. Gao, Z. Pan, M. A. Shook, and D. Li, 2020: Diurnal climatology of planetary boundary layer height over the contiguous United States derived from AMDAR and reanalysis data. *J. Geophys. Res. Atmos.*, **125**, e2020JD032803, https://doi.org/10.1029/2020JD032803.

Zoogman, P., D. J. Jacob, K. Chance, L. Zhang, P. Le Sager, and A. M. Fiore, 2009: Using geostationary observations to improve ozone air quality forecasts. *2009 Fall Meeting*, San Francisco, CA, Amer. Geophys. Union, Abstract A51M-08.